ICT-based Understanding of Spinal Cord Networks with Applications to Spinal Cord Injuries

by

Meltem Civaş

A Dissertation Submitted to the
Graduate School of Sciences and Engineering
in Partial Fulfillment of the Requirements for
the Degree of

Master of Science

in

Electrical and Electronics Engineering

KOÇ
UNIVERSITY

September, 2018

ICT-based Understanding of Spinal Cord Networks with Applications to Spinal Cord Injuries

Koç University

Graduate School of Sciences and Engineering

This is to certify that I have examined this copy of a master's thesis by

Meltem Civaş

and have found that it is complete and satisfactory in all respects,
and that any and all revisions required by the final
examining committee have been made.

Committee Members:

_____

Prof. Özgür B. Akan

_____

Prof. Fatih Alagöz

_____

Prof. Alper T. Erdoğan

Date: _____

To my parents

ABSTRACT

Research efforts in nanotechnology have opened the way for deployment of nanonetworks comprising nanomachines with bio-inspired capabilities inside the body. Deploying nanonetworks and connecting them to the Internet based on Internet of Bio-Nano Things (IoBNT) framework can result in wide range of possible biomedical applications including treatments techniques of nervous diseases. Molecular communication (MC) has been proposed as a communication technology solution to be employed among nanomachines. Since biological systems use most advanced forms of MC, this motivates information and communication technology (ICT) community to develop bio-inspired communication systems at the nanoscale for nervous system diseases such as spinal cord injuries (SCI), which cannot be recovered to the date by any treatment method. In this respect, a framework was proposed for developing ICT-based treatment and diagnosis tools for nervous diseases. According to this framework, understanding of nervous nanonetworks and extracting ICT metrics based on their analysis are the key steps for the development of these techniques. Hence, this thesis focuses on the realistic modeling and information theoretical analysis of spinal cord networks. To this end, we apply existing neuro-spike communication channel models to the particular spinal cord networks to analyze the rate of information flow across them. Based on our analysis, we obtain correlations between several types of spinal injuries and information theoretical metrics. Moreover, we further propose novel ICT-based treatment techniques which can use the advantages aspects of existing and bio-inspired communication & networking methods to recover disrupted communications in the nervous nanonetwork after SCI.

ÖZETÇE

Nano teknoloji alanındaki çalışmalar, nano makinelerden oluşan nano ağların vücut içinde kullanılmalarının yolunu açmıştır. Nano ağların kullanımı ve Biyo-Nano nesnelerin interneti çatısı altında internete bağlanması, sinir sistemi hastalıkları tedavileri dahil sayısız biyomedikal uygulamalarla sonuçlanabilir. Moleküler haberleşme (MH), nano makineler arasında kullanım için önerilmiş bir haberleşme teknolojisidir. Biyolojik sistemlerin MH'nin en gelişmiş yöntemlerini kullanması, bilgi ve iletişim teknolojileri (BT) topluluğunu omurilik yaralanmaları (OY) gibi tedavisi olmayan sinir sistemi hastalıklarını nano düzeyde ve biyolojiden ilham alan tedavi yöntemleri geliştirmeye yöneltmektedir. Bu konuda, sinir sistemi hastalıklarını BT temelli tedavi ve teşhis yöntemleri geliştirmek için bir çatı önerilmiştir. Bu çatıya göre, sinir ağlarının anlayışı ve analizlerinden BT metriklerinin elde edilmesi bu tekniklerin geliştirilmesinde önemli faktörlerdir. Bu nedenle, bu tez omurilik ağlarının gerçekçi modellenmesi ve bilgi kuramı analizine eğilmektedir. Bu amaçla, haberleşme hızını analiz etmek için mevcut nöro atım haberleşme kanal modellerini omurilik ağına uygulamaktayız. Analizimi dayanarak, çeşitli omurilik yaralanmaları ve bilgi kuramı metrikleri arasında korelasyonlar elde etmekteyiz. Ayrıca, OY'den sonra bozulan sinir sistemi ağındaki haberleşmeyi yeniden sağlamak için mevcut ve biyo-ilhamlı ağ oluşturma & haberleşme tekniklerinin avantajlarını kullanabilen özgün BT temelli tedavi yöntemleri önermekteyiz.

ACKNOWLEDGMENTS

I would like to express my deepest gratitude and sincere thanks to my advisor Dr. Özgür Barış Akan for his everlasting guidance, encouragement and tolerance. Without his support, it would be impossible to complete this thesis.

I would like to thank to Dr. Fatih Alagöz and Dr. Alper Tunga Erdoğan for taking part in my thesis committee and for their valuable suggestions and comments.

I want to thank to all members of Next-generation and Wireless Communications Laboratory (NWCL) for their collaboration, constant help and friendship. I specially want to thank Dr. Hamideh Ramezani for her valuable comments.

I would also like to acknowledge the support of Koç University, which made the completion of this thesis possible.

I wish to thank my parents and my brother for motivating and encouraging me throughout my study. I would also like to thank Merve for her invaluable support and friendship. Finally, I am grateful to my friends Hazan, Nafi and Seyhan for their support.

TABLE OF CONTENTS

LIST OF TABLES

LIST OF FIGURES

Chapter 1

INTRODUCTION

1.1 ICT-based Understanding of Spinal Cord Networks and the Treatment of Spinal Cord Injuries

Advancements in nanotechnology have enabled the deployment of nanonetworks comprising of nanomachines with biologically inspired capabilities inside human body. In this respect, nanonetwork paradigm opens the way for wide range of applications including biomedical applications relying on Internet of Bio-Nano Things (IoBNT) framework which was proposed as the basis for such systems [4].

To realize nanonetworks, one of the most promising technologies is molecular communication (MC) because many types of MC are already being employed by biological systems inside us [5]. Considering the evaluation of our biological systems, communication between bio-nano entities is expected to be optimized in the nanoscale while certain limitations exists such as processing, memory and energy source. Intra-body nanonetworks are parts of our biological systems and they include the examples of most advanced forms of MC such as electro-chemical signaling between neurons in the very large scale nervous nanonetwork, namely, neuro-spike communication. This motivates the development of nanoscale bio-inspired communication systems for information and communication technology (ICT) based treatment and diagnosis of nervous system dysfunctions such as spinal cord injuries (SCI).

SCI disrupts healthy communication between the brain and the spinal cord (SC), which is sustained by spinal cord pathways, and results in serious motor and sensory deficits in the subjects due to injured or lost pathways. To recover these pathways,

bio-engineering, medical and surgical methods have been developed; however, to the date recovery from SCI is not possible by any means of treatment and biological recovery. On the other hand, ICT-based treatment techniques can be successful at recovering SCI by benefiting from the existing and bio-inspired communication, networking techniques and applying these methods to recover healthy communication in the injured SC network. On the other hand, this requires understanding of healthy and damaged nervous nanonetworks from ICT perspective. In this respect, framework for the development of future ICT-based treatment techniques and tools was introduced in [5]. Accordingly, extensive research effort has focused on the modeling and analysis of neuro-spike communication [6–12] and other physical and conceptual communication models for neural communication [13–17]. However, realistic neuro-spike communication network model for SC, which can enable us to determine characteristics of healthy and damaged SC network using ICT metrics, has not been considered, yet.

Therefore, the focus of this thesis is information theoretical understanding of spinal cord networks/injuries and the development of further ICT-based treatment methods for recovering SCI. Thus, in Chapter 2, we model a spinal cord motor circuitry that is responsible from the control of a particular muscle by applying multi-terminal neuro-spike network model to determine the total rate of information flow to the spinal cord for the movement of a muscle and investigate the correlation between information theoretical metrics and SCI. In Chapter 3, we extend our single-hop neuro-spike model in Chapter 2 to obtain more realistic analysis of brain-spinal cord information transmission through descending spinal cord pathways. The deduced results from our analysis can be used in diagnosis tools relying on nanonetwork simulation frameworks and in developing deployment strategies for replacement intra-body nanonetworks. Finally, in Chapter 4, we propose two novel ICT-based treatment methods for SCI and discuss their future applications.

1.2 Main Contributions

Regarding ICT-based understanding of nanoscale communication in the nervous nanonetwork and treatment methods for SCI, main contributions of this thesis are listed as follows.

- Realistic treatment of a spinal cord motor nucleus system by application of single-hop multi-terminal neuro-spike network model and performing it analysis with the realistic channel parameters.
- Deriving the upper bound for the network capacity of layered neuro-spike communication networks modeling the spinal cord descending pathways.
- Deducing relationship between several information theoretical metrics and upper motor neuron syndromes and lower motor neuron syndromes, respectively.
- Proposing novel ICT-based treatment techniques that can recover disrupted sensory and motor transmission after SCI by either bypassing injury site or replacing injured neurons.

1.3 Thesis Outline

This thesis is organized as follows.

Chapter 2: In this chapter, we consider a spinal cord motor nucleus controlling a particular muscle, which is a basic motor network in the spinal cord. Hence, it is an an ideal candidate for studying in order to have an understanding of spinal cord injuries (SCI). When communication fails through a particular motor nucleus, its effects can be monitored directly on the corresponding muscle. Typical spinal cord motor nucleus system contains pool of lower motor neurons (MNs) controlling a muscle by integrating synaptic inputs from spinal interneurons (INs), upper motor neurons (DNs) and sensory neurons (SNs). We consider spinal cord motor nucleus system from ICT perspective with the aim of quantifying the rate of information flow

across it. To this end, we model an equivalent single-hop multi-terminal network, where multiple transmitting nodes representing heterogeneous population of DNs, INs and SNs send information to multiple receiving nodes corresponding to MNs. To identify the outputs at receiving nodes, we define corresponding neuro-spike communication channel and then find the bound on total rates across this network. Based on the network model, we analyze achievable rates for a particular motor nucleus system called Tibialis Anterior (TA) motor nucleus in the spinal cord numerically and simulate several spinal cord dysfunction scenarios. The numerical results reveal that decrease in the maximum total rates with the lower motor neuron injury causes weakness in the affected muscle.

Chapter 3: In this chapter, we extend our single-hop neuro-spike network model to layered neuro-spike network model with the focus of its application to descending spinal cord pathway, which is responsible from down-link transmission of brain motor signals to the spinal cord. Our aim is to analyze the rate of motor information flow to the spinal cord. To this end, we model the spinal cord motor network as layered network consisting of cascade of two independent neuro-spike X-channels. Since the network capacity is determined by the minimum hop capacity, we formulate the capacity for neuro-spike X-channel and derive upper bound for it. Moreover, based on our evaluations, we reach to several deductions between information theoretical metrics and upper/lower motor neuron syndromes.

Chapter 4: In this chapter, we propose two ICT-based treatment techniques for SCI. The first proposal is based on neural interface systems (NIS), where external machines are interfaced with the brain and the spinal cord such that signals from the brain are directly routed to the limbs for movement. Our proposed system can provide fine motor movement by restoring sensory communication pathway unlike the existing neural interfaces. The second proposal relates to the design of artificial neurons that can be used to replace the injured or dead neurons. ICT-based techniques can provide successful outcome by utilizing highly evolved communication and networking methods developed to the date. In addition to treatment capability, proposed methods

can enable smart health care for the patients with SCI by Internet of Bio-Nano Things (IoBNT) applications. Furthermore, NISs can also be interfaced with the Internet of Everything (IoE) environment so that direct interaction between the brain and the things is enabled.

Chapter 2

INFORMATION THEORETICAL ANALYSIS OF MULTI-TERMINAL NEURO-SPIKE NETWORKS IN SPINAL CORD

2.1 Introduction

Spinal cord system comprises of complex networks including motor circuits, which involve in execution of motor actions such as locomotion and postural control by integrating inputs from periphery neurons and brain. Spinal motoneurons, MNs, are the final common pathway where whole information is resolved. Spinal cord motor system consists of several motor nuclei each of which having group of MNs controlling a particular muscle group [1]. When the communication fails through a particular motor nucleus, its effects can be monitored directly on the corresponding muscle. Main synaptic inputs to a typical motor nucleus system are conveyed from the periphery via SNs, from the brain via DNs as illustrated in Fig. 2.1. Moreover, INs relay inputs from the spinal cord to MNs.

In the literature, brain and neurons of spinal cord have been modeled as cloud and fog nodes based on the analogy between cloud and fog networking architecture in [15]. In [14], to recover communication failures through spinal cord sensory pathways, replacement neural network using time division multiple access has been proposed. However, a realistic communication network model for spinal cord system taking physiological characteristics of neurons into account is not considered in the literature to our knowledge.

In this chapter, our aim is to quantify the bound on the information flow across a spinal cord motor nucleus system. To this end, we model equivalent neuro-spike

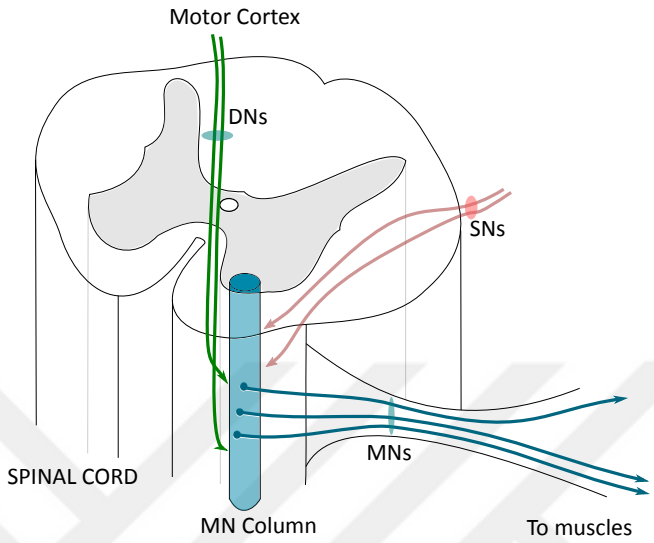

Figure 2.1: Spinal cord motor nucleus system

communication network to a motor nucleus system as a single-hop multi terminal network consisting of multiple transmitting and receiving nodes corresponding to pre-synaptic and post-synaptic neurons, respectively. The inputs to the equivalent channel are spike trains transmitted by the transmitting nodes and the outputs are spike trains generated at the receiving nodes. Utilizing the neuro-spike communication model describing vesicle release from pre-synaptic neuron, post-synaptic filtering and post-synaptic spike generation, we find the output at each receiving node. Using this, we derive a bound on the total achievable rate across the network. Based on the neuron quantities in the spinal cord TA motor nucleus as shown in Table 3.4 and realistic biophysical channel parameters for each class of neurons in the system, we analyze effects of different class of pre-synaptic and post-synaptic neurons on the total maximum achievable rates.

The main motivation behind this chapter is finding relationship between the information theoretical metrics and several spinal cord dysfunctions. Hence, we simulate several spinal cord diseases by changing the number of receiving and transmitting nodes. Then, we find relations between information theoretical metrics and spinal cord dysfunctions. The results reveal that when part of MNs is injured, decreasing

Table 2.1: Types of Excitatory (Ex) and Inhibitory (Inh) Neurons (TA motor nucleus) [1]

Class of Neuron	**Ex/Inh**	**Quantity**
SN (Ia afferent)	Ex	280
IN (Ib interneuron)	Inh	350
IN (Ia interneuron)	Inh	350
MN (S, FF, FR)	-	350

total maximum rate results in weakness in the muscle. These results may help in designing ICT-based diagnosis and treatment techniques. To our knowledge, this is the first work studying a spinal cord system from neuro-spike communication perspective.

The rest of the chapter is organized as follows. Section 2.2 describes the equivalent network model for spinal cord motor nucleus. In Section 2.3, bound on the total rate across the network is formulated. In Section 2.4, numerical results are discussed.

2.2 Neuro-spike Communication Network Model of the Motor Nucleus System

We consider a single-hop multi-terminal neuro-spike communication network, where M transmitting nodes want to send information to K receiving nodes. Thus, transmitting nodes only transmit, whereas receiving nodes only receive. Transmitting nodes represent heterogeneous population of pre-synaptic SNs, INs, DNs. Receiving nodes correspond to post-synaptic MNs. A simple multi-terminal neuro-spike network is shown in Fig. 2.2.

Transmitted input spike train to the channel, S_i, is associated with transmitting node i, where $i \in \mathcal{M} = \{1, 2, .., M\}$. We assume that inputs to the channel are independent. The spike train output of the channel Y_j is associated with receiving node j, where $j \in \mathcal{K} = \{1, 2, .., K\}$. Transmitting node i sends information to receiving node j at rate R_{ij}. The channel is memoryless with the channel transition function $P(Y^{\mathcal{K}}|S^{\mathcal{M}}) = P(Y_1, Y_2, ..., Y_K|S_1, S_2, ..., S_M)$.

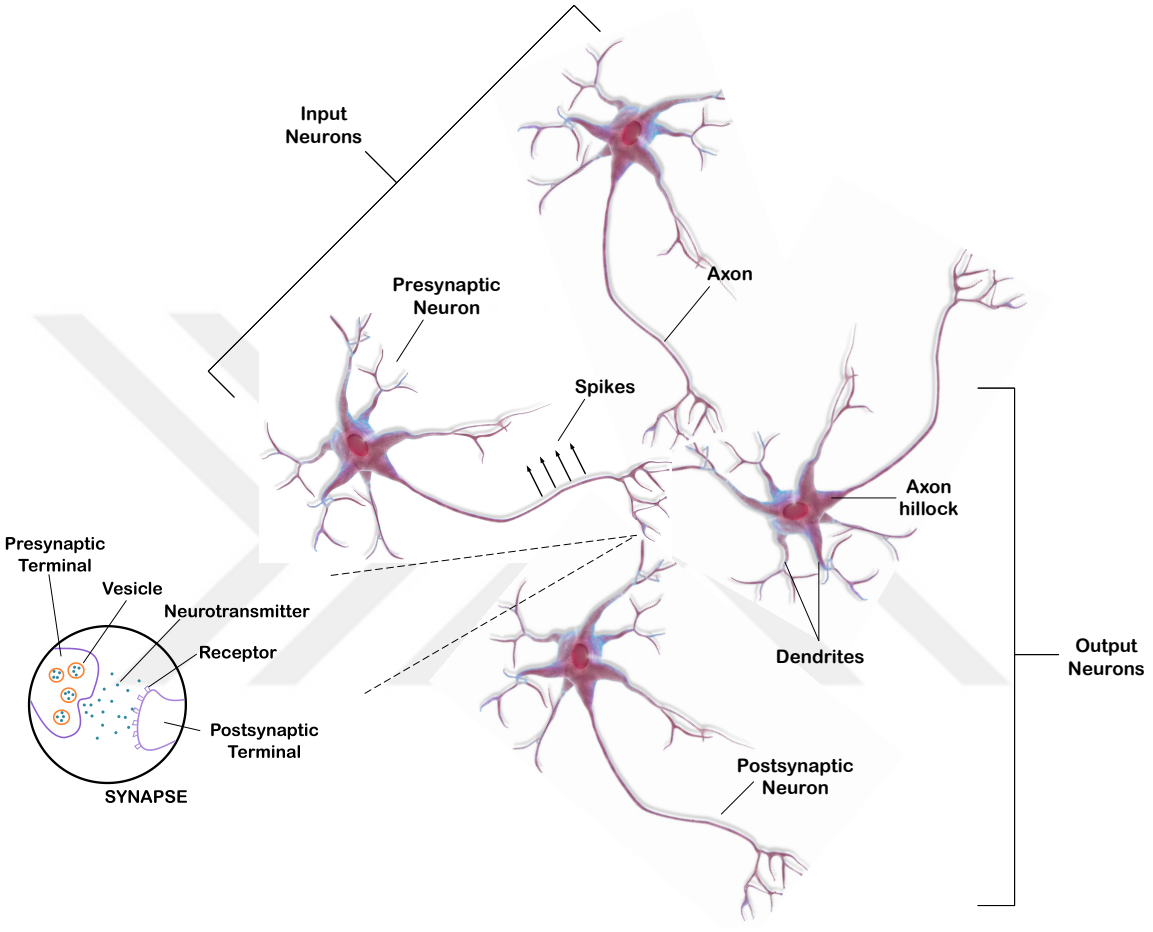

Figure 2.2: Neuro-spike multi-terminal network

The channel considered is illustrated in Fig. 2.3. Possible links in the network are {SN→MN, IN→MN, DN→MN}. Each class of link is under a connectivity probability. $p_{\mathrm{SM}}, p_{\mathrm{IM}}$ and p_{DM} denote connectivity probabilities for {SN→MN, IN→MN, DN→MN}, respectively. The connectivity matrix, $\mathbf{X} = [X_{i,j}]$ contains connectivity state of each class of links. Accordingly, $X_{i,j}$ takes value of 1 if the synaptic connection exists and takes 0 otherwise for each $i \in \mathcal{M}$ and $j \in \mathcal{K}$.

In order to derive the outputs accessed by the receiving nodes, we first need to define inputs to the channel given in Fig. 2.3 and then describe the channel model. Inputs and outputs of the channel are utilized in finding the bound on the total rate of information flow across the network. For point-to-point links in the network, we

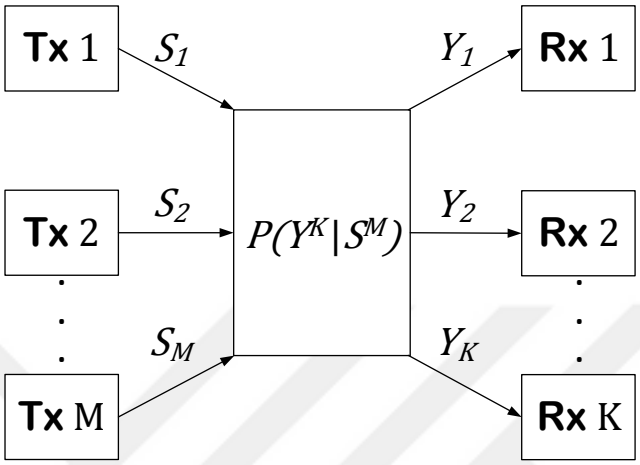

Figure 2.3: Considered one-hop multi-terminal network consisting of transmitting (left) and receiving nodes (right)

use existing neuro-spike channel blocks in the literature [6–12, 18] that are applicable to the spinal cord synapses.

Neuro-spike communication channels comprise of cascade stages, namely, axonal transmission, vesicle release, post-synaptic filtering and spike generation at the post-synaptic neuron. Pre-synaptic terminal refers to the part of pre-synaptic neuron where vesicles are released. Vesicles contain chemical substances called neurotransmitters, which diffuse through a specialized gap called synaptic cleft. Reaching post-synaptic terminal, neurotransmitters bind to the receptors located there, which generate potential at the post-synaptic membrane. When the membrane potential reaches the threshold value, the output spike is generated at the post-synaptic neuron. In the following parts, we describe the neuro-spike channel model under consideration which is illustrated in Fig. 2.4 and derive the outputs at receiving nodes.

2.2.1 Pre-synaptic Inputs

Transmitting node or pre-synaptic neuron i generates Poisson spike train, $S_i(t)$, with rate λ_i, where $i \in \mathcal{M}$. For each neuron, λ_i is constrained such that $0 \leq \lambda_i \leq \lambda_{\max,i}$, where $\lambda_{\max,i}$ is maximum firing rate of the pre-synaptic neuron i. The limitation on the

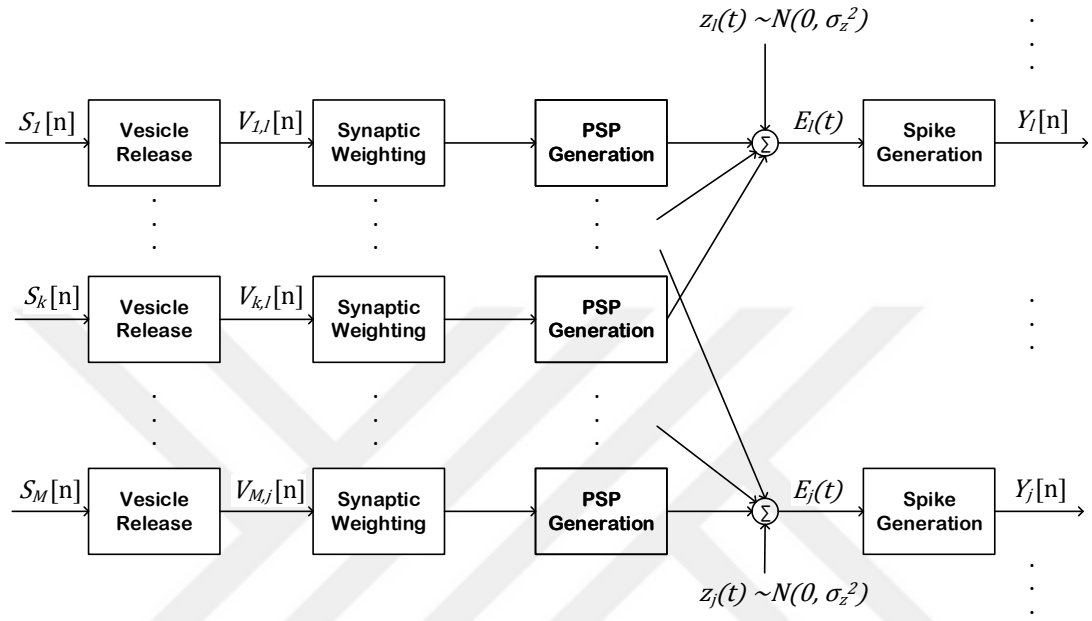

Figure 2.4: Detailed diagram of the channel

firing rate arises from *refractory period*, which is the minimum time period between any successive spikes [19]. Thus, time window can be divided into small windows with the length of Δt such that at most one spike can occur in Δt [10]. Therefore, probability of a spike in the nth time window is $P\{S_i[n] = 1\} = 1 - \exp(\lambda_i \Delta t)$. Spike train then propagates to pre-synaptic terminal, where vesicle release takes place, through the axon. Axonal transmission is considered reliable [20].

2.2.2 Vesicle Release

Probability of vesicle release from a release site is governed by available vesicles for release in the pool-based model [21]. Since dynamic synapses are not in the scope of this chapter, we assume that size of readily releasable pool at a release site is constant. We adopt the term *functional contact* to refer any vesicle release sites associated with a pre-synaptic neuron as used in the [22]. From each functional contact of a typical IN, SN and DN, at most one vesicle is released when a spike arrives to a pre-synaptic terminal [23, 24]. Moreover, typical IN, SN and DN can make multiple functional

contacts with post-synaptic MN [23, 25].

Considering the transmission from transmitting node i to receiving node j, the probability of a vesicle release at a single functional contact upon the arrival of a spike during nth time window is $P_{\text{rel},i} \triangleq P\{V_{i,j}[n] = 1 | S_i[n] = 1\}$. In case of multiple independent functional contacts, probability of k vesicle releases from T_i functional contacts follows Poisson binomial distribution [11, 12] as described by the following equation.

$$P\{V_{i,j}[n] = k | S_i[n] = 1\} = \frac{1}{T_i + 1} \sum_{l=0}^{T_i} F^{-lk} \prod_{m=1}^{T_i} (1 + (F^l - 1) P_{i,m}), \tag{2.1}$$

where $F = \exp(\frac{2\sqrt{-1}\pi}{T_i+1})$ and $P_{i,m}$ is the probability of release from mth functional contact of ith pre-synaptic neuron.

2.2.3 Post-synaptic Filtering

Neurotransmitter binding to post-synaptic receptors increases or decreases the membrane potential depending on the type of synapses. Thus, excitatory post-synaptic potential (EPSP) and inhibitory post-synaptic potential (IPSP) are generated at the post-synaptic neuron in excitatory and inhibitory synapses, respectively. Inhibitory and excitatory types of pre-synaptic neurons are shown in Table 2.1. Moreover, in {DN→MN} links, excitatory synapses occur.

Post-synaptic potential filtering at receiving node or post-synaptic neuron j due to access from transmitting node i is described by alpha function [7] as follows.

$$e_{i,j}(t) = w_{i,j} h_p \frac{t}{t_p} \exp(1 - \frac{t}{t_p}), t \geq 0 \tag{2.2}$$

where h_p and t_p are peak quantal amplitude and time to rise peak, respectively. $w_{i,j}$ is the weighting variable representing synaptic strength between transmitting node i and receiving node j. Values of quantal amplitude and rising time depend on the type of synapse. Thus, for the excitatory synapses, we define $h_p = h_{\text{ex}}$ and $t_p = t_{\text{ex}}$, whereas for the inhibitory synapses $h_p = h_{\text{inh}}$ and $t_p = t_{\text{inh}}$.

Synaptic strengths are characterized by morphology of synapses such as distribution of number of synapses and pre-synaptic terminal sizes [26]. Combined effect manifests itself as *lognormality*, which is reported for spinal cord motor circuits [27]. Thus, w, follows lognormal distribution with probability density function

$$f(w|\mu,\sigma) = \frac{1}{w\sigma\sqrt{2\pi}} \exp\left(\frac{-(\log w - \mu)^2}{2\sigma^2}\right); w > 0 \tag{2.3}$$

where $\mu = \log(\frac{m^2}{\sqrt{v+m^2}})$ is log mean and $\sigma = \sqrt{\log(\frac{v}{m^2+1})}$ is log variance, given m and v are mean and variance, respectively. w_{SM}, w_{IM} and w_{DM} are the lognormal random variables with corresponding mean and variance pairs $(m_{\mathrm{SM}}, v_{\mathrm{SM}})$, $(m_{\mathrm{IM}}, v_{\mathrm{IM}})$ and $(m_{\mathrm{DM}}, v_{\mathrm{DM}})$ defined for each link in the set of synaptic links {SN→MN, IN→MN, DN→MN}, respectively.

2.2.4 Spike Generation

Membrane potential, $E_j(t)$, at receiving node j is spatiotemporal summation of contributions from each synaptic access in terms of EPSP and IPSP. Membrane potential is given by

$$\begin{aligned} E_j(t) = \theta_0 &+ \sum_{l\in\{\mathrm{SN}\}} \sum_{t_n \le t} w_{\mathrm{SM},l,j} X_{l,j} V_{l,j}[n] h_{p,\mathrm{ex}}(t - t_n) \\ &+ \sum_{i\in\{\mathrm{IN}\}} \sum_{t_n \le t} w_{\mathrm{IN},i,j} X_{i,j} V_{i,j}[n] h_{p,\mathrm{inh}}(t - t_n) \\ &+ \sum_{m\in\{\mathrm{DN}\}} \sum_{t_n \le t} w_{\mathrm{DN},m,j} X_{m,j} V_{m,j}[n] h_{p,\mathrm{ex}}(t - t_n) + z_j(t), \end{aligned} \tag{2.4}$$

where t_n is the beginning of nth time window. {SN}, {IN} and {DN} are the sets of SNs, INs and DNs in $\mathcal{M}$, respectively. $h_{p,\mathrm{ex}}(t) = h_{\mathrm{ex}} \exp(1 - \frac{t}{t_{\mathrm{ex}}})$ and $h_{p,\mathrm{inh}}(t) = h_{\mathrm{inh}} \exp(1 - \frac{t}{t_{\mathrm{inh}}})$ are EPSP and IPSP filters, respectively. θ_0 is the resting membrane potential and $z_j(t)$ is white Gaussian synaptic noise with variance σ_z^2. When $E_j(t)$ reaches the spiking threshold, θ_j, the post-synaptic neuron fires a spike, i.e., $Y_j[n] = 1$.

2.3 Bound on the Achievable Rates

In this part, we derive the bound on total achievable rates across the network using the cut-set bound.

We are given a cut $(\mathcal{M}, \mathcal{K})$. That is, nodes are already partitioned into two disjoint sets, namely, the set of transmitting nodes $\mathcal{M}$ consisting of SN, IN and DN nodes and the set of receiving nodes $\mathcal{K}$ consisting of MN nodes. By the defined cut, the channel reduces to multiple input multiple output (MIMO) channel so that total information flow from $\mathcal{M}$ to $\mathcal{K}$ is bounded by the rate MIMO channel can support [28]. Thus, cut-set bound on the information flow from M transmitting nodes to K receiving nodes is given by the following [29].

$$\sum_{i\in\mathcal{M}, j\in\mathcal{K}} R_{ij} \leq I(S^{\mathcal{M}}[n]; Y^{\mathcal{K}}[n]), \tag{2.5}$$

where $S^{\mathcal{M}}[n] = \{S_1[n], S_2[n], ..., S_M[n]\}$ is the set of input spike trains to the channel and $Y^{\mathcal{K}}[n] = \{Y_1[n], Y_2[n], ..., Y_K[n]\}$ is the set of output spike trains at the nth time interval. $\{R_{ij}\}$ are achievable rates from transmitting node i to receiving node j and the bound is maximized over joint input distribution $p(S^{\mathcal{M}}[n])$. On the other hand, we know that the input spike trains, $S_i[n]$, are independent and Poisson distributed with λ_i. Thus, the right hand side in (2.5) is maximized over λ_i's.

Considering the channel model and the number of neurons, simulation of network scenario is highly complex. Thus, we perform numerical analysis of the network in the next section based on the following assumptions:

- Same class of neurons have identical biophysical properties, i.e., identical spiking rate, probability of release and number of functional contacts.

- All functional contacts of a pre-synaptic neuron are identical, i.e., $P_{i,m} = P_{\text{rel},i}, \forall m \in [1, T_i]$. Thus, vesicle release process reduces to Binomial release $B(T_i, P_{rel,i})$.

Therefore, number of output spikes at the receiving nodes depends only on the number of transmitted spikes by transmitting nodes. By the definition, mutual information is

$$I(S^{\mathcal{M}}[n]; Y^{\mathcal{K}}[n]) = H(Y^{\mathcal{K}}[n]) - H(Y^{\mathcal{K}}[n]|S^{\mathcal{M}}[n]), \tag{2.6}$$

As a result of aforementioned assumptions, the conditional entropy in (2.6) is derived as

$$H(Y^{\mathcal{K}}[n]|S^{\mathcal{M}}[n]) = H(\sum_{i=1}^{K} Y_i[n] = s_m | \sum_{l=1}^{M} S_l[n] = s_s) \tag{2.7}$$

where s_m is number of output spikes at receiving nodes and s_s corresponds to number of input spikes transmitted by transmitting nodes.

2.4 Numerical Analysis

In this section, we evaluate performance of the network numerically with respect to maximum total achievable rate and mutual information. Based on the numerical results obtained, we discuss the spinal cord dysfunctions and the information theoretical metrics.

Probability of release is generally low (less than 0.3) at central synapses [24], thus, we use $p_D = 0.3$ for probability of release from DN. Moreover, we adopt $p_{\mathrm{DM}} = 0.9$ based on the evidences that MNs have common projections from the brain [30]. Remaining parameters are given in Table 2.2.

Throughout the simulations, unless otherwise stated, we assume that spiking activity occurs during a motor action, for which SNs and INs are spiking at mean rates of $\lambda_{\mathrm{SN}} = 80$ Hz [31] and $\lambda_{\mathrm{IN}} = 20$ Hz [32], respectively. Number of different class of neurons that are given in Table 3.4 are used in the simulations unless otherwise stated. Number of SNs, INs, DNs and MNs recruited in the network are denoted by $N_{\mathrm{SN}}, N_{\mathrm{IN}}, N_{\mathrm{DN}}, N_{\mathrm{MN}}$, respectively.

Table 2.2: Model and simulation parameters

Parameter	**Symbol**	**Value**
Spiking Threshold (MN)	θ	-46.02 mV [33]
Resting Potential (MN)	θ_0	-64.81 mV [33]
Noise standard deviation	σ_z	0.1 mV [7]
Discretization time step	Δt	4 ms [10]
Spike width	Δt_s	4 ms [10]
Functional contact (SN,IN)	T_S, T_I	$8, 7$ [34, 35]
Probability of release (IN)	p_I	0.5 [36]
Probability of release (SN)	p_S	0.5
Peak quantal EPSP	h_{ex}	0.1 mV [37]
Peak quantal IPSP	h_{inh}	-0.08 mV [36]
Time to peak of EPSP	t_{ex}	0.2 ms [34]
Time to peak of IPSP	t_{inh}	0.2 ms [38]
Connectivity: IN to MN	p_{IM}	0.2 [30]
Connectivity: SN to MN	p_{SM}	0.8 [39]
Mean of w (SN, IN, DN)	$m_{\text{SN}}, m_{\text{IN}}, m_{\text{DN}}$	1 [30]
Variance of w (SN, IN, DN)	$v_{\text{SN}}, v_{\text{IN}}, v_{\text{DN}}$	1 [30]

In the following part, we first analyze effects of number of lower motor neurons, MNs, on the maximum total achievable rate when the mutual information is simulated for different spiking rates of DNs, λ_{DN}. Secondly, we evaluate effects of number of DNs, upper motor neurons, and number of functional contacts per DN, T_D, on the maximum total achievable rate.

2.4.1 Maximum Total Rate versus Number of MNs

Fig. 2.5a shows mutual information versus λ_{DN} for different number of MNs. Around $\lambda_{\text{DN}} = 120$ Hz, mutual information is at the maximum. This value is comparable to the reported maximum spiking rate of DNs, that is $\lambda_{\text{DN,max}} \sim 106$ Hz (corticospinal pyramidal cells) [40]. Moreover, maximum total rate increases with the number of MNs, N_{MN}, as shown in Fig. 2.5b. With $N_{\text{MN}} = 350$, which is the quantity referring to the TA nucleus as given in Table 3.4, bound on the total rate is ~ 1.3 bits per network use.

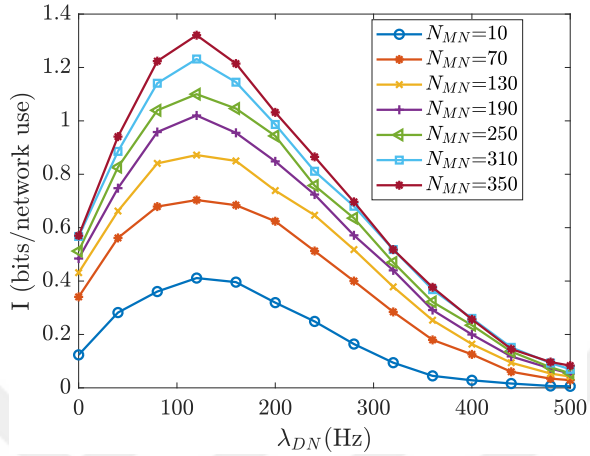

(a) $N_{DN} = 100, T_D = 8$

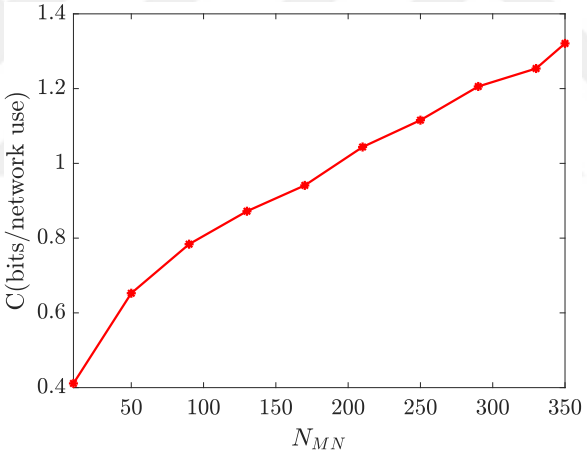

(b) $N_{DN} = 100, T_D = 8$

Figure 2.5: (a) Mutual information and (b) maximum total achievable rates for different number of MNs.

General design considerations with regard to synaptic nanonetworks include that multiterminal network capacity can be increased with number of receiving nodes deployed in the network, considering the result depicted in Fig. 2.5b.

2.4.2 Maximum Total Rate versus Number of DNs

In this part, we analyze the effect of number of upper motor neurons, DNs, on maximum total achievable rate across the network so that we can quantify changes on total achievable rates with the upper motor neuron loss. We lack of data regarding

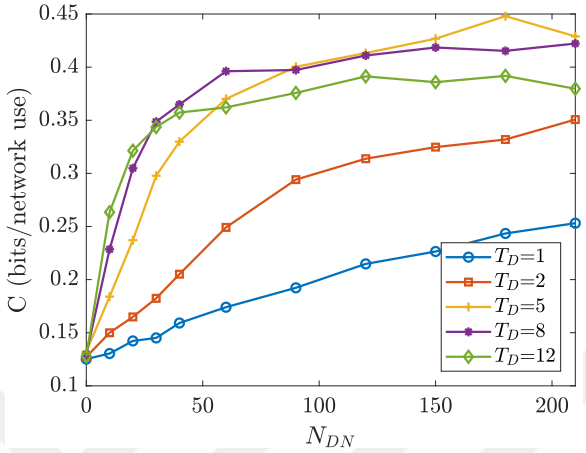

(a) $N_{MN} = 10$

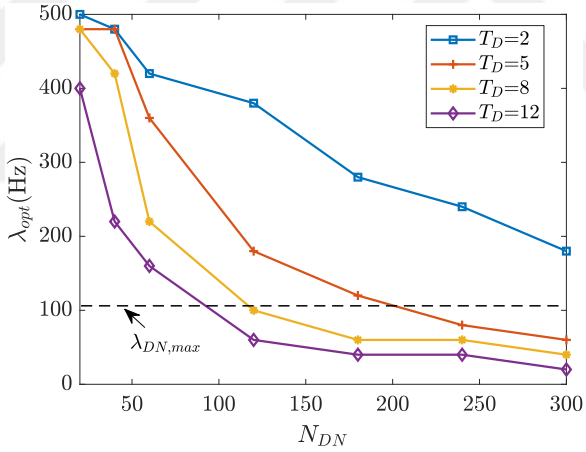

(b) $N_{MN} = 10$

Figure 2.6: (a) Maximum achievable total rate for different number of functional contacts per DN and (b) optimal spiking rates

average number of functional contacts, T_D, in {DN $\rightarrow$ MN} links and number of DNs projecting to TA nucleus. Thus, maximum total rate is simulated for different T_D and N_{DN} values. Maximum total rates are obtained with respect to different spiking rates of DN, λ_{DN}'s, with the maximum of 500 Hz.

Fig. 2.6a shows the maximum total rate of flow of information across the network in the allowable spiking range. As depicted in Fig. 2.6a, maximum total information rate across the network increases with the number of upper motor neurons, N_{DN}, up to a point and then show saturation trend. Moreover, as the number of functional

contacts per DN, T_D, increases, maximum total rate that can be attained increases in low N_{DN} range ($\sim$ 0 to 40 DNs). This is expected because maximum of the mutual information is not reached in the low N_{DN} range ($\sim$ 0 to 40 DNs) in case of low T_D's (1 to 2 T_D's). The result also reveals that in the low T_D range, the network is more prone to capacity decrease when part of upper motor neurons is lost as a result of SCI. Moreover, with relatively lower T_D's, higher maximum total rate can be obtained when high number of DNs such as 200 DNs are recruited in the network. This result is not observable for the cases $T_D = 1, 2$ because higher number of DNs is needed to reach maximum of the mutual information.

Optimal λ_{DN} values achieving maximum total rate are shown in Fig. 2.6b. When maximum firing rate constraint, i.e., $\lambda_{\mathrm{DN}} \leq \lambda_{\mathrm{DN,max}}$, is applied, maximum total rates are not achievable in low T_D range in any case due to the physical limitations on the firing rate.

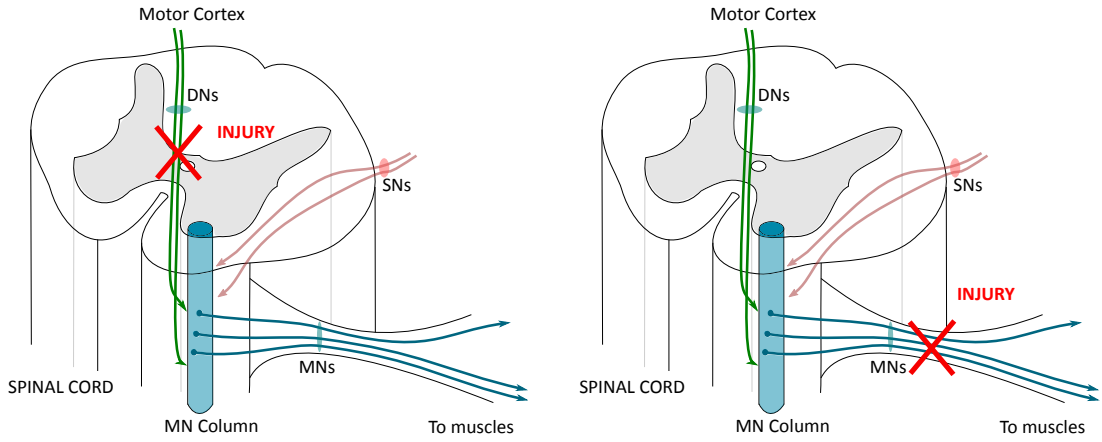

(a) Upper Motor Neuron Injury (b) Lower Motor Neuron Injury

Figure 2.7: Illustration of types of SCI considered

2.4.3 Information Theoretical Metrics and Spinal Cord Dysfunctions

In this part, we deduce the relation between the results obtained via numerical simulations and several reported symptoms of spinal cord dysfunctions which are illustrated in Fig. 2.4.2. The relation between observed symptoms of the spinal cord injuries and

information theoretic metrics, such as maximum total rate and mutual information, can provide an insight regarding communication failures through the spinal cord due to injuries or diseases. Aforementioned metrics may be used in ICT-based diagnosis tools and treatment techniques for SCI.

Loss of lower motor neurons, i.e., MNs, can arise from neurodegeneretive diseases such as amyotrophic lateral sclerosis (ALS) or damage to the cells because of SCI. One of the most profound symptoms of MN loss is weakness in the associated muscle [19]. As illustrated in Fig. 2.5b, decrease in total maximum rate with decreasing number of MNs is resulting in the weakness in the muscle affected from the injury.

As shown in Fig. 2.6a, maximum total rate of information flow is not affected significantly from partly loss of DNs or upper motor neurons up to a critical number of neuron loss, when DNs have relatively high number of functional contacts. This result is compatible with intrinsic mechanisms of the nervous system evolved to cope with communication failures, in a way that nervous system can compensate the loss of neurons with the exception of cell loss in significant extent by increasing redundancy in the form of functional contact [41] via plasticity. After critical number of cell loss, however, motor actions cannot be performed normally [42].

Chapter 3

RATE OF INFORMATION FLOW ACROSS LAYERED NEURO-SPIKE NETWORKS IN SPINAL CORD

3.1 Introduction

Research effort on the deployment of nanonetworks inside body and connecting them to Internet of Bio-Nano Things (IoBNT) environment [4, 5] opens the way for wide range of possible applications including ICT-based treatment and diagnosis for SCI. On the other hand, understanding of spinal cord networks in healthy and diseased conditions from ICT-perspective needs to be established to realize these treatment methods.

Neuro-spike communication is one of the bio-compatible communication techniques proposed to be employed among replacement nano-entities to recover the disrupted spinal cord network after SCI. Most studies regarding neuro-spike communication have been focused on realistic modeling and analysis of physical channels at various complexity levels [6–12,18]. In these studies, neurons are generally assumed to be cortical neurons. On the other, communication among distinct populations of neurons in the spinal cord network is not considered.

In this chapter, we consider the spinal cord network which is responsible from the down-link transmission of motor signals from the brain to spinal cord. Since our aim is to investigate the rate of motor information flow to the spinal cord, we treat concurrent sensory transmission to the spinal cord as interference. The spinal cord motor network is abstracted as cascade of two independent neuro-spike channels.

Therefore, achievable sum rates across the network is bounded by the minimum cut capacity. Deriving exact cut capacity can be cumbersome so that we derive upper bound for it. Simulation results show that upper bound can be tight depending on the number of neurons recruited in the network.

The rest of this chapter is organized as follows. In Section 3.2, biophysical description of spinal cord motor pathway is given. In Section 3.3, we model spinal cord motor pathway as two-hop neuro-spike communication network and formulate its information capacity. In Section 3.4, we describe single-hop neuro-spike channel model and in Section 3.5, we derive cut set bound for this channel. In Section 3.6, performance of the network is evaluated by simulations. Next, in Section 3.7, we deduce a relationship between spinal cord injuries and information theoretical metrics based on our analysis.

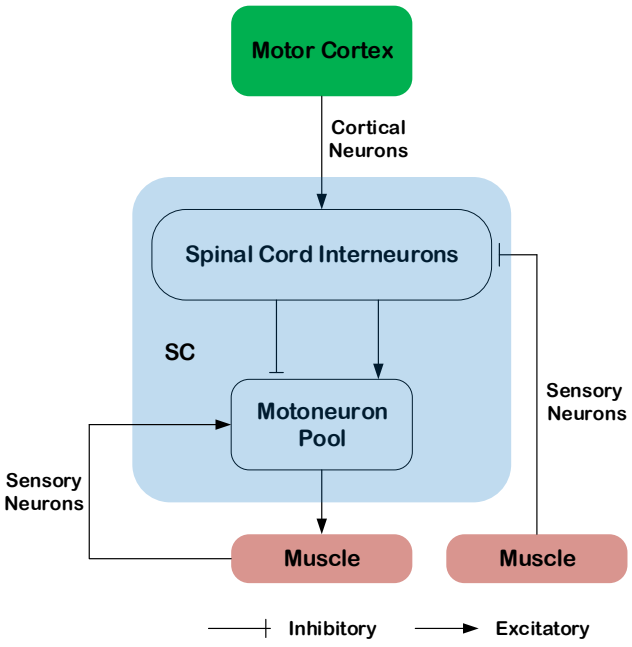

Figure 3.1: Down-link transmission of brain motor commands to the spinal cord (SC)

3.2 Physical Description of Spinal Cord Network

Overall nervous network consists of peripheral nervous network (PNN) and central nervous network (CNN) [43]. A main part of PNN, which is called somatic nervous network (SNN), controls voluntary body movements by conveying sensory inputs to CNN from the body via sensory nerves and transmitting motor outputs to skeletal muscles via motor nerves. CNN, on the other hand, comprises of two main centers which are the brain and spinal cord. The brain generates motor response that is to be transmitted to the spinal cord. Spinal cord integrates motor and sensory information coming from the brain and PNN, respectively and generates motor output, which is transmitted to the muscles. In this chapter, we particularly consider spinal cord network associated with SNN, whose failure cam result in loss of movement.

Spinal cord communication pathways comprise of sensory and motor pathways. Sensory pathways formed by sensory nerves perform uplink transmission of sensory information from skeletal muscles to the brain. Sensory transmission route passes through spinal cord and reaches several destinations in the brain. Motor route involves in downlink transmission of motor commands from the brain to muscles. Motor information generated by neuronal sources in the brain is transmitted to spinal cord by bundle of nerve fibers called descending tracts. In the spinal cord, received inputs are processed and relayed to muscles. Spinal cord has 31 spinal segments, each of which contains two pairs of nerve roots where nerves enter to or leave from the spinal cord. From dorsal root, sensory neurons (SN) conveying information from muscles enter to spinal cord where they make synapse with spinal cord neurons. The spinal cord neurons either transmit sensory information to brain following ascending sensory route or relay it to spinal cord motoneurons (MN). Axons of MNs residing in the spinal cord leave the spinal cord from the ventral root and innervate muscles. MNs which are located at a spinal cord segment form clusters which are called motor nucleus. Each motor nucleus is associated with a particular muscle and constitutes the final destination for motor information.

For instance, a motor nucleus innervates a particular muscle as shown in Fig. 2.1. Therefore, union of motor nuclei in a spinal segment is an important parameter with regard to down-link information capacity of the spinal cord network. In this chapter, we particularly focus on down-link information transmission from brain to the spinal cord through descending pathways. In the following part, we describe transmission through descending spinal route in detail.

3.2.1 Down-link Transmission Through Descending Spinal Cord Pathways

Down-link transmission of brain motor commands to muscles follows the route that is illustrated in Fig. 3.1. To demonstrate, let us consider the delivery of brain's motor commands to motor nucleus A. Cortical neurons (CN) located in motor cortex encode motor commands into spikes which are transmitted to the spinal cord via long axons of CNs. In the spinal cord, axons of CNs deliver motor signals to destination MNs residing in motor nucleus A via relay spinal interneurons (IN). In primates, CNs also directly project to MNs [44]. However, since most of physiological data is collected from non-primates such as rodent, we consider the spinal system in the context of no direct connection between CN and MN. Finally, MNs in motor nucleus A innervate muscle A. Besides, MNs receive direct sensory inputs from SNs as well as indirect sensory inputs from antagonist muscle, let us say muscle B, via relay INs [1]. Hence, MNs are the final destination of multiple dependent and independent signals from descending spinal cord route (and also partly from sensory pathways) considering the fact that they receive inputs from SNs, INs and CNs, simultaneously.

3.3 Spinal Cord Pathways as Layered Neuro-Spike Communication Networks

In this section, we describe multi-terminal neuro-spike network model of spinal cord motor pathway and formulate the expression for the capacity of motor information transmission from the brain to the spinal cord.

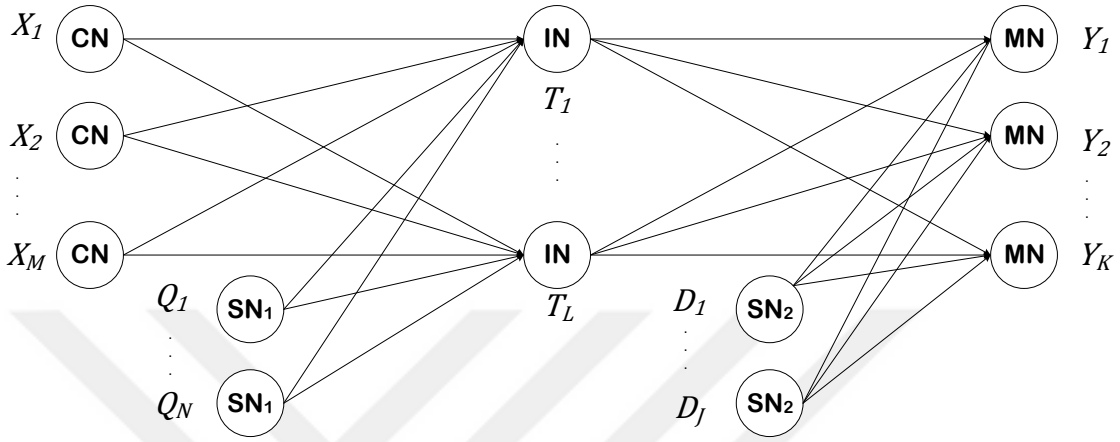

Figure 3.2: Spinal cord layered network

3.3.1 Capacity of Spinal Cord Motor Network

Motor commands of the brain are relayed to MNs via spinal INs as aforementioned in Section 3.2. Considering a single motor nucleus, the system can be modeled as layered network with two-hops where relay nodes retransmit decoded information to the destination nodes. Thus, transmit nodes only transmit and receive nodes only receive, whereas relay nodes have both receive and transmit capabilities.

The information transmission is in the forward direction as illustrated in Fig. 3.2. In the first layer, source CN nodes located in the brain and source SN nodes from antagonist muscle transmit their inputs $X_1, ..., X_M, Q_1, ..., Q_L$ to the destination IN nodes. Inputs from source nodes are assumed to be mutually independent. Relay IN nodes, which are working cooperatively, retransmit the channel outputs $T_1, T_2, ..., T_L$ to destination MN nodes in the second layer.

The network is cascade of two independent X-channels, since the output at a node in particular layer only depends on the inputs transmitted by nodes in the adjacent layer in the backward direction. The cascaded channels are defined by the following channel transition probabilities:
$p(T_1, ..., T_L|X_1, ..., X_M, Q_1, ..., Q_N)$, $p(Y_1, ..., Y_K|T_1, ..., T_L, D_1, ..., D_J)$.

The capacity is limited by the minimum hop capacity [45].

IN and MN nodes receive direct inputs from different SN nodes which are denoted by $(Q_1, ..., Q_N)$ and $(D_1, ..., D_J)$, respectively. However, SN nodes are not associated with any CN node as illustrated in Fig. 3.2. That is, they are not involved in the transmission of cortical information to the spinal cord. Hence, interference due to access of SN nodes to the channels is treated as noise. Accordingly, bound on the sum rate capacity is then given by the following.

$$\begin{aligned} C &= \min\left\{ \max_{p(X^M|Q^N)p(Q^N)} I(X^{\mathcal{M}}; T^{\mathcal{L}}|Q^{\mathcal{N}}), \max_{p(T^{\mathcal{L}}|D^{\mathcal{J}})p(D^{\mathcal{J}})} I(T^{\mathcal{L}}; Y^{\mathcal{K}}|D^{\mathcal{J}}) \right\} \\ &= \min\left\{ \max_{p(X^M|Q^N)p(Q^N)} I_1, \max_{p(T^{\mathcal{L}}|D^{\mathcal{J}})p(D^{\mathcal{J}})} I_2 \right\} \\ &\overset{(a)}{=} \min\left\{ \max_{p(X^M)p(Q^N)} H(T^{\mathcal{L}}|Q^{\mathcal{N}}) - H(T^{\mathcal{L}}|Q^{\mathcal{N}}, X^{\mathcal{M}}), \right. \\ &\left. \max_{p(T^{\mathcal{L}})p(D^{\mathcal{J}})} H(Y^{\mathcal{K}}|D^{\mathcal{J}}) - H(Y^{\mathcal{K}}|D^{\mathcal{J}}, T^{\mathcal{L}}) \right\} \\ &= \min\{C_1, C_2\}, \end{aligned} \tag{3.1}$$

where (a) follows from that all sources are mutually independent.

3.4 Single-Hop Neuro-spike Network

In this section, we first describe the channel model of general neuro-spike X-channel in the spinal cord. Then, we formulate the cut set bound for the channel. Based on this, we can find single hop capacities, C_1 and C_2, which are given by (3.1).

3.4.1 Neuro-spike X-channel in Spinal Cord

In a multi-terminal neuro-spike communication network, M transmitting nodes want to send information to K receiving nodes. In our case, transmitting nodes have only transmit and receiving nodes only receiving capabilities. Regarding spinal cord network, M sources generally comprise of heterogeneous population of pre-synaptic neurons and K destination nodes can be either population of post-synaptic INs or MNs.

As illustrated in Fig. 2.3, ith source node transmits input spike train X_i, $i \in \mathcal{M} = \{1, 2, .., M\}$ to the channel. The output at jth destination node is Y_j, $j \in \mathcal{K} = \{1, 2, .., K\}$. Thus, the channel is defined by channel transition probability $P(Y^{\mathcal{K}}|X^{\mathcal{M}}) = P(Y_1, Y_2, ..., Y_K|X_1, X_2, ..., X_M)$. Moreover, ith source node sends information to the jth destination node at the rate of R_{ij}.

Connectivity between source and destination nodes, $\mathbf{Z} = [Z_{i,j}]$, is governed by connection probabilities between each type of pre-synaptic and post-synaptic neurons. Accordingly, $Z_{i,j} = 1$ with probability $p_{c,i,j}$ and $Z_{i,j} = 0$ otherwise for each $i \in \mathcal{M}$ and $j \in \mathcal{K}$. In general, every source neuron does not have connection with every destination neuron. Therefore, we assume that a link with zero capacity exists between unconnected nodes so that the channel becomes an X-channel.

3.4.2 Channel Model

The channel model is based on general neuro-spike communication channel as given in [18]. Since diffusion and binding processes are mostly reliable [8], they are ignored. Rather, synaptic strength is modeled as a random variable. Moreover, *functional contact* refers to any vesicle release site associated with a pre-synaptic neuron as used in [22]. From each functional contact of a typical IN, SN and DN, at most one vesicle is released when a spike arrives to a pre-synaptic terminal [23, 24]. In addition, typical IN, SN and DN have multiple functional contacts associated with a post-synaptic neuron [23, 25]. Thus, pre-synaptic neurons are presumed to have multiple functional contacts in the spinal cord. Channel model under consideration is described briefly as follows.

- X_i is input to the channel which is transmitted by ith pre-synaptic neuron and defined as Poisson arrival of a spike with λ_i in a time window Δt.

- Probability of vesicle release from T_i functional contacts when a spike exists at the pre-synaptic terminal follows Poisson binomial distribution [11, 12] as

described by the following equation.

$$P\{V_{i,j}[n] = k | X_i[n] = 1\} = \frac{1}{T_i + 1} \sum_{l=0}^{T_i} F^{-lk} \prod_{m=1}^{T_i} (1 + (F^l - 1)P_{i,m}), \quad (3.2)$$

where $F = \exp(\frac{2\sqrt{-1}\pi}{T_i+1})$ and $P_{i,m}$, $m \in [1, T_\mathrm{i}]$, is probability of release from mth functional contact at pre-synaptic neuron i. When functional contacts of the neuron are assumed to be identical, i.e., $P_{i,m} = P_{\mathrm{rel},i}, \forall m \in [1, T_i]$, vesicle release process is described by binomial distribution $\mathrm{B}(T_i, P_{rel,i})$.

- Postsynaptic potential generation is modeled as alpha function [7] as given by

$$h_{i,j}(t) = \gamma_{i,j} h_p \frac{t}{t_p} \exp(1 - \frac{t}{t_p}), t \geq 0 \quad (3.3)$$

where h_p is peak quantal EPSP and IPSP amplitude and t_p time to rise peak. $\gamma_{i,j}$ is defined as follows.

$$\gamma_{i,j} = \begin{cases} 1 & \text{if } i \to j \text{ is EXC,} \\ -1 & \text{if } i \to j \text{ is INH,} \end{cases}$$

where EXC and INH denote excitatory and inhibitory synapses, respectively.

- Synaptic strengths are affected by synapse morphology such as distribution of synapses and pre-synaptic terminal sizes [26]. Joint effect exhibits lognormal response in spinal cord motor circuits as reported in [27]. Therefore, synaptic strength due to a release of a single vesicle, W, follows lognormal distribution with probability density function (pdf) given by

$$f_W(w) = \frac{1}{w\sigma\sqrt{2\pi}} \exp\left(\frac{-(\ln w - \mu)^2}{2\sigma^2}\right); w > 0 \quad (3.4)$$

where $\mu = \ln(\frac{m^2}{\sqrt{v+m^2}})$ is log mean and $\sigma = \sqrt{\ln(\frac{v}{m^2+1})}$ is log variance, given m and v are mean and variance, respectively.

Considering a single neuro-spike link $(i \to j)$, conditioned on $V_{i,j}[n] = v_{i,j}$, post-synaptic response is weighted by sum of lognormal variables, i.e., $B_{i,j} = \sum_{l=1}^{v_{i,j}} W_l$, where $W_l \sim \ln \mathcal{N}(\mu_l, \sigma_l)$. Using Fenton-Wilkinson approximation [46], $B_{i,j}[n]$ is approximated as lognormal, i.e., $B_{i,j} \approx e^{\nu}$, where $\nu \sim \mathcal{N}(\mu_\nu, \sigma_\nu^2)$. Mean and variance are given as follows.

$$\begin{aligned} \mu_\nu &= \ln\left(\sum_{l=1}^{v_{i,j}} \exp(\mu_l + \frac{\sigma_l^2}{2})\right) - \frac{\sigma_\nu^2}{2} \\ \sigma_\nu^2 &= \ln\left(\frac{\sum_{l=1}^{v_{i,j}} \exp(2\mu_l + \sigma_l^2)(\exp(\sigma_l^2) - 1)}{(\sum_{l=1}^{v_{i,j}} \exp(\mu_l + \frac{\sigma_l^2}{2}))^2}\right) \end{aligned} \tag{3.5}$$

- Total post-synaptic potential at the jth receiving node is then described by the following equation [18].

$$G_j(t) = \theta_{0j} + \sum_{i=1}^{M} \sum_{t_n \le t} B_{i,j} \gamma_{i,j} h_{i,j}(t - t_n) + s_j(t), \tag{3.6}$$

where θ_{0j} is the resting membrane potential and $s_j(t)$ is white Gaussian synaptic noise with variance σ_s^2. Spike is generated if $G_j(t) > \theta_j$, where θ_j is spiking threshold at the jth receiving node.

3.5 Cut Set Bound for Single Hop Neuro-spike Network

According to the cut-set bound for general multiterminal networks [29], cut separates the source nodes from the destination nodes such that nodes are divided into two disjoint sets Ω and Ω^c. Thus, the capacity region of the neuro-spike X-network is

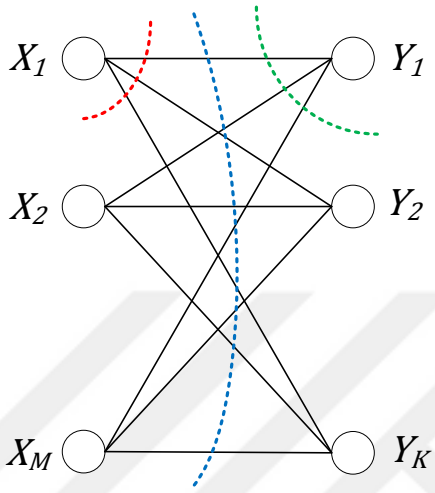

Figure 3.3: Cuts in the channel considered [3]

contained in the set of rates that satisfies the following.

$$\sum_{i\in\Omega, j\in\Omega^c} R_{ij} \leq \max_{p(X_1,...,X_M)} I(X^{\Omega}; Y^{\Omega^c}|X^{\Omega^c}), \tag{3.7}$$

for all $\Omega \subset \{1, ..., M\}$. $\{R_{ij}\}$ is the set of achievable rates. $p(X_1, ..., X_M)$ is given as joint Poisson distribution with mutually independent $X_i \sim Poisson(\lambda_i)$, where $i \in [1, M]$. Thus, right hand side in (3.7) is maximized over λ_i's [18].

In general X-networks, two types of cut exists: Cuts separating single node from the other nodes and cuts separating multiple sources from the receiving nodes [3]. Regarding the latter, cut capacity $C_\Omega = \max_{p(X_1,...,X_M)} I(X^{\Omega}; Y^{\Omega^c}|X^{\Omega^c})$ is the capacity of multiple-input multiple-output (MIMO) channel. Using cut capacity, we can find the bound on the rate of information flow from a particular population of pre-synaptic neurons to the population of post-synaptic neurons. Deriving exact cut capacity, C_Ω, could be cumbersome; however, we can decompose it in a way that it would be the sum of bounds on multiple-input single-output (MISO) channels. Thus, we can derive a loosened bound as follows.

$$
\begin{aligned}
&I(X^{\Omega};Y^{\Omega^c}|X^{\Omega^c}) \\
&\quad = H(Y^{\Omega^c}|X^{\Omega^c}) - H(Y^{\Omega^c}|X^{\Omega^c}, X^{\Omega}) \\
&\quad = H(Y^{\Omega^c}|X^{\Omega^c}) - H(Y^{\Omega^c}|X^{\mathcal{M}}) \\
&\quad = H(Y^{\Omega^c}|X^{\Omega^c}) - \sum_{i\in\Omega^c} H(Y_i|X^{\mathcal{M}}, Y_{i-1}, ..., Y_1) \\
&\quad \overset{(a)}{=} H(Y^{\Omega^c}|X^{\Omega^c}) - \sum_{i\in\Omega^c} H(Y_i|X^{\mathcal{M}}) \\
&\quad \overset{(b)}{\leq} \sum_{i\in\Omega^c} H(Y_i|X^{\Omega^c}) - H(Y_i|X^{\mathcal{M}}) \\
&\quad = \sum_{i\in\Omega^c} I(X^{\Omega}; Y_i|X^{\Omega^c})
\end{aligned}
\tag{3.8}
$$

where (a) follows from that given all inputs, the outputs are independent because each neuro-spike communication link is independent from the others and (b) follows from the independence bound on the entropy. Thus, bound on cut capacity is given by

$$C_{\Omega} \leq C_{\Omega}^{\text{up}} = \max_{p(X_1,...,X_M)} \sum_{i\in\Omega^c} I(X^{\Omega}; Y_i|X^{\Omega^c}). \tag{3.9}$$

Similarly, the sum rate satisfies the following.

$$\sum_{i=1}^{M}\sum_{j=1}^{K} R_{i,j} \leq \max_{p(X_1,...,X_M)} I(X^{\mathcal{M}}; Y^{\mathcal{K}}). \tag{3.10}$$

Mutual information in the right hand side of (3.10) is given by

$$I(X^{\mathcal{M}}; Y^{\mathcal{K}}) = H(Y^{\mathcal{K}}) - H(Y^{\mathcal{K}}|X^{\mathcal{M}}). \tag{3.11}$$

Accordingly, conditional entropy is given as follows.

$$\begin{aligned} H(Y^K|X^M) &= \sum_{\underline{x}} H(Y_1,...,Y_K|X^{\mathcal{M}}=\underline{x})P(X^{\mathcal{M}}=\underline{x}) \\ &\overset{(a)}{=} \sum_{\underline{x}}\sum_{j=1}^{K} H(Y_j|X^{\mathcal{M}}=\underline{x})P(X^{\mathcal{M}}=\underline{x}). \end{aligned} \tag{3.12}$$

where (a) follows from the fact that given all inputs the outputs are independent since all neuro-spike links in the network are independent.

Based on [18], the conditional entropy is given as follows.

$$\begin{aligned} P\{Y_j[n]=1|X^M=\underline{x}\} &= P\{G_j(t)>\theta_j|X^M=\underline{x}\} \\ &= \sum_{\underline{v}_j}\prod_{i=1}^{M} P\{V_{i,j}[n]=v_{i,j}|X_i[n]=x_i\} \\ &\quad P(s_j(t_n+t_p)>\theta_j-\theta_{0j}-\sum_{i=1}^{M}\sum_{l=1}^{v_{i,j}} W_{i,j,l}\gamma_{i,j}h_p|V_j^M=\underline{v}_j), \end{aligned} \tag{3.13}$$

where $V_j^M=\{V_{1,j},...,V_{M,j}\}$ and corresponding realizations $\underline{v}_j=\{v_{1,j},...,v_{M,j}\}, v_{i,j}\in[0,T_i]$.

For full excitatory connections, i.e, $\gamma_{i,j}=1 \quad \forall i\in M, j\in K$, such as the first layer in the motor path, the expression can be further reduced as follows. Let us define $L_{i,j}=h_pW_{i,j,l}$. Hence, $L_{i,j}\sim \ln\mathcal{N}(\mu_{i,j,l}+\ln(h_p),\sigma^2_{i,j,l})$. Sum of indepedent lognormal random variables $\sum_{i=1}^{M}\sum_{l=1}^{v_{i,j}} L_{i,j}$ can be approximated as a new lognormal random variable $A_j\sim e^{\nu_j}$, where $\nu_j\sim\mathcal{N}(\mu_{\nu_j},\sigma_{\nu_j})$ so that pdf of A_j, $f_A(a)$, can be expressed as given in (3.4) [47].

Based on Fenton-Wilkinson approximation [46], μ_{ν_j} and σ_{ν_j} are given as follows.

$$\mu_{\nu_j} = \ln\left(\sum_{i=1}^{M}\sum_{l=1}^{v_{i,j}} \exp(\mu_{i,j,l} + \ln(h_p) + \frac{\sigma_{i,j,l}^2}{2})\right) - \frac{\sigma_{\nu_j}^2}{2},$$
$$\sigma_{\nu_j}^2 = \ln\left(\frac{\sum_{i=1}^{M}\sum_{l=1}^{v_{i,j}} \exp(2(\mu_{i,j,l} + \ln(h_p) + \sigma_{i,j,l}^2)(\exp(\sigma_{i,j,l}^2) - 1)}{\left(\sum_{i=1}^{M}\sum_{l=1}^{v_{i,j}} \exp(\mu_{i,j,l} + \ln(h_p) + \frac{\sigma_l^2}{2})\right)^2}\right). \tag{3.14}$$

Let χ_j be the sum of independent $s_j(t_n + t_p)$ and A_j. Then, (3.13) is restated as

$$P\{Y_j[n] = 1 | X^M = \underline{x}\} = \sum_{\underline{v}_j}\prod_{i=1}^{M} P\{V_{i,j}[n] = v_{i,j} | X_i[n] = x_i\} P(\chi_j > \theta_j - \theta_{0j} | V_j^M = \underline{v}_j) \tag{3.15}$$

Since $s_j(t_n + t_p)$ and A_j are independent, pdf of χ_j can be found as

$$f_\chi(z) = \int_{-\infty}^{\infty} f_S(t) f_A(z - t)\mathrm{d}t. \tag{3.16}$$

Closed form expression for $f_\chi(z)$ is not present; however, it can be computed numerically. Moreover, $P(\chi_j \leq \theta_j - \theta_{0j} | V_j^M = \underline{v}_j)$ can be found by conditional pdf of χ_j, i.e., $f_\chi = f_S \circledast f_{A|V}$, where $f_{A|V}(a|\underline{v}) = \dfrac{\partial}{\partial A} P(A \leq a | V_j^M = \underline{v})$ and $\circledast$ denotes convolution. Thus, $P\{Y_j[n] = 1\}$ can be computed from the following expression.

$$P(\chi_j > \theta_j - \theta_{0j}) = 1 - \sum_{\underline{v}_j} P(\chi_j \leq \theta_j - \theta_{0j} | V_j^M = \underline{v}_j) P\{V_j^M = \underline{v}_j\}. \tag{3.17}$$

Simulating exact sum capacities could be prohibitive because of high number of neurons in the spinal cord. Thus, in the next section exact capacities are simulated based on the assumption that same type of neurons have identical properties such as probability of vesicle release, number of functional contacts. Moreover, all functional contacts of a neuron is assumed to be identical. Therefore, conditional entropy reduces

to the following.

$$H(Y^{\mathcal{K}}|X^{\mathcal{M}}) = H(\sum_{i=1}^{K} Y_i[n] = s_t| \sum_{j=1}^{M} X_j[n] = s_q), \tag{3.18}$$

where s_t and s_q are total number of spikes at the receiving nodes and transmitting set of nodes, respectively.

3.6 Performance Evaluations

In this section, we analyze the effects of number of transmitting or receiving nodes and sensory interference on the capacity or the rate of information flow across the spinal network abstracted by the model presented in Section 3.3.

For the simulations, we are based on characteristic classes of neurons in a motor nucleus [1] corresponding to each type of nodes in the network model illustrated in Fig. 3.2. Accordingly, IN nodes comprise excitatory interneurons denoted by ExIN and inhibitory Ia interneurons (IaIN). Ia neurons associated with antagonist muscle correspond to SN_1 nodes in the network, whereas Ia neurons exciting MNs are represented by SN_2 nodes in the network. CN population considered to be descending tracts neurons conveying motor commands to the spinal cord through INs. We assume that connectivity matrix $\mathbf{Z}$ is given since connections between neurons in the spinal cord are already established naturally. Thus, synaptic connections are assigned beforehand based on $\mathbf{Z}$ which is formed by random permutations according to the connectivity probabilities given in Table 3.2. Two types of INs (IaIN and ExIN) are assumed to have same biophysical properties. Similarly, all neuron properties are assumed to be identical across a particular type of neuron population such as SN, MN or CN population. Regarding spinal cord circuitry, we neglect Renshaw cells, which carry feedback from MN itself to MN, since feedback does not increase capacity of a neuro-spike channel that we consider because PSP generation in a time interval does not effect the spike generation in the subsequent interval in our setting. Moreover, we assume that IPSP and EPSP amplitudes at a post-synaptic neuron is independent

Table 3.1: Model and simulation parameters

Parameter	**Symbol**	**Value**
Spiking Threshold (MN)	θ_{MN}	-46.02 mV [33]
Resting Potential (MN)	θ_0	-64.81 mV [33]
Spiking Threshold (IN)	θ_{IN}	-32.2 mV [48]
Resting Potential (IN)	θ_0	-46.4 mV [48]
Noise standard deviation	σ_z	0.1 mV [7]
Discretization time step	Δt	4 ms [10]
Spike width	Δt_s	4 ms [10]
Peak quantal PSP	h_{p}	0.1 mV
Time to peak of PSP	t_{p}	0.2 ms
Mean of $W\ \forall i, j$	m	1 [30]
Variance of $W\ \forall i, j$	v	1 [30]

from the type of pre-synaptic neuron. Thus, values of PSP amplitude and time to rise peak are fixed. Considering channel parameters, number of functional contacts T is fixed to a value that is in the corresponding range for a particular synaptic connection given in Table 3.3. Unless otherwise stated, $T = 8$ for IN $\rightarrow$ MN, $T = 4$ for CN $\rightarrow$ IN, values of probability of release are as given in Table 3.3 and number of neurons are as given in Table 3.4. Remaining parameters are given in Table 3.1.

Table 3.2: Connectivity

Class of Neuron	p_c
Ia $\rightarrow$ MN	0.8 [39]
Ia(Antagonist) $\rightarrow$ IaIN	0.7 [39]
IaIN $\rightarrow$ MN	0.15 [39]
ExIN $\rightarrow$ MN	0.3
CN $\rightarrow$ ExIN	0.65 [49]
CN $\rightarrow$ IaIN	~ 0.20 [49]

3.6.1 Capacity of Brain-Spinal Cord Neuro-spike Channel

We lack of data regarding number of CNs projecting to INs, N_{CN}. Thus, upper bound and exact cut capacities are simulated for increasing number of CNs for the first layer which is given in Fig. 3.2.

Table 3.3: Number of Functional Contacts

Class of Neuron	**Functional Contacts**	P_{rel}
IaIN $\rightarrow$ MN	$\sim 4-11$ [49]	0.5
CN $\rightarrow$ IN	$\sim 2-6$ [49]	0.3
SN_2 (Ia) $\rightarrow$ MN	~ 8 [37]	0.5
SN_1 (Ia-Antagonist) $\rightarrow$ IN	6	0.5

Fig. 3.4a shows C_1 and C_1^{up} for increasing N_{CN} and various number of excitatory and inhibitory INs ratios. According to this, sum rate capacity increases with the number of CN nodes, N_{CN} with a rate that decreases with N_{CN}. After a point increasing N_{CN} does not change the capacity significantly. I_1 given by (3.1) can be written as $I(X^{\mathcal{M}};T^{\mathcal{L}}|Q^{\mathcal{N}}) = I(T^{\mathcal{L}}|Q^{\mathcal{N}},X^{\mathcal{M}}) - I(T^{\mathcal{L}}|Q^{\mathcal{N}})$. When high number of transmitting CN nodes exist, the spike generation at receiving IN nodes is mostly due to cortical inputs so that the effect of sensory interference is less. Because of this, $I(T^{\mathcal{L}}|Q^{\mathcal{N}})$ term does not change significantly with N_{CN}. Hence, the effect of $I(T^{\mathcal{L}}|Q^{\mathcal{N}})$ on $I(X^{\mathcal{M}};T^{\mathcal{L}}|Q^{\mathcal{N}})$ for increasing number of cortical inputs is insignificant. Thus, $I(T^{\mathcal{L}}|Q^{\mathcal{N}},X^{\mathcal{M}})$ term is related with the increase in capacity because of higher dependence of output spikes to the cortical inputs.

As shown in Fig. 3.4a, with higher $N_{\text{ExIN}}/N_{\text{IaIN}}$, capacity reaches higher values. This trend can be explained with different connectivity levels between pre-synaptic CN-SN populations and post-synaptic excitatory/inhibitory IN populations. That is, $p_c(CN \rightarrow ExIN) > p_c(CN \rightarrow IaIN)$ and $p_c(SN_1 \rightarrow IaIN) > p_c(SN_1 \rightarrow ExIN) = 0$ as given in Table 3.2. For instance, since SN_2 nodes densely project to $IaIN$ nodes, the effect of sensory interference on the capacity is more when $N_{ExIN}/N_{IaIN} = 1/2$ compared to the case $N_{ExIN}/N_{IaIN} = 2$. Moreover, for lower N_{ExIN}/N_{IaIN} or N_{IaIN}/N_{ExIN}, capacity upper bound C_1^{up} is tight; however, for high N_{ExIN}/N_{IaIN} or N_{IaIN}/N_{ExIN} values, the bound is loose, which is again related with the effect of sensory information transmission on the rate of motor information flow as a result of distinct connectivity levels between several types of transmitting and receiving nodes.

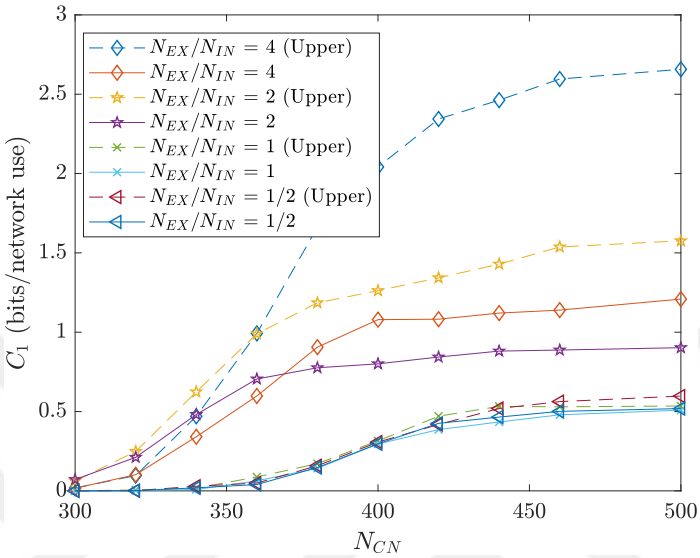

(a) $N_{SN_1} = 50$, $\lambda_{SN} = 50$ Hz, N_{IaIN}, $N_{EXIN} \in \{5, 10, 20\}$

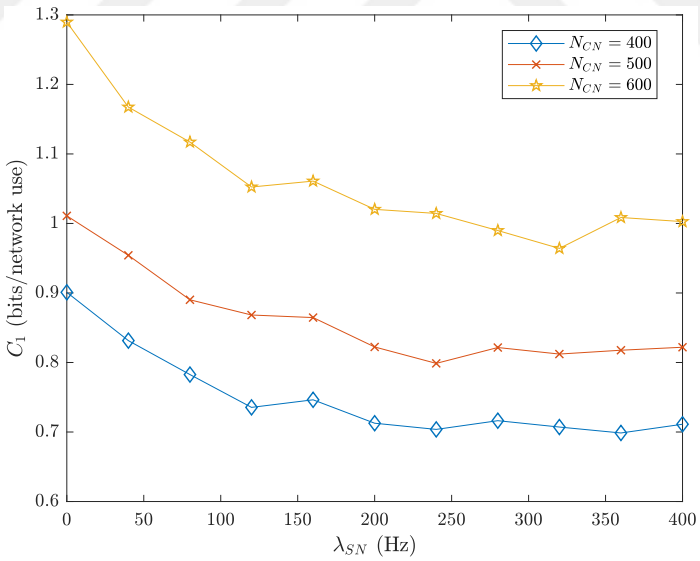

(b) $N_{CN} = 400, N_{SN_1} = 50, , N_{IaIN} = 5, N_{EXIN} = 10$

Figure 3.4: Sum capacity of first layer (C_1) for different values of (a) number of source CN nodes, N_{CN} and (b) λ_{SN}. Capacity is found over λ_{CN} ranged from 0 to 500 Hz.

The effect of sensory interference on the capacity of channel is also demonstrated in Fig. 3.4b. Cut capacity, C_1, reaches maximum when sensory interference does not present, i.e., $\lambda_{SN_1} = 0$ Hz as expected. On the other hand, as λ_{SN_1} increases, C_1 decreases with decreasing rate and then reaches a constant level. Moreover, C_1 is higher if more number of CN nodes N_{CN} are recruited. This follows from the

observation that C_1 increases with N_{CN} as shown in 3.4a.

3.6.2 Capacity and Rate of Interneuron-Motoneuron Channel

In this part, we analyze the effect of number of receiving MN nodes N_{MN} on the channel capacity of second layer C_2 and the effect of sensory interference on the mutual information I_2 which is given by (3.1). In this case, capacity is found by maximizing I_2 over firing rates of transmitting IN nodes λ_{IN}'s with the exception of inhibitory IN nodes (IaINs) whose firing rates are fixed.

N_{MN} is one of the independent parameters affecting the network capacity. Fig. 3.5a shows maximum rate of information flow from IN nodes to MN nodes for various number MN nodes when sensory interference is introduced. C_2 increases with N_{MN} at a decreasing rate. Thus, recruiting few more MN nodes when relatively small number of MN nodes exist in the network will improve C_2 significantly; however, the converse will result in slight improvement in C_2. This result is especially important for lower motor neuron diseases treatment, since in such disease conditions receiving MN nodes can decrease in number.

Level of sensory interference limits the rate of motor information transmission. Thus, we investigate I_2 for several values of spike firing rate of SN nodes, λ_{SN_2}. As shown in Fig. 3.5b, maximum of mutual information I_2 is lower when λ_{SN_2} is higher. Accordingly, bound on the sum rate of motor information flow is at the maximum when $\lambda_{SN_2} = 0$, i.e., sensory interference does not present. Moreover, firing rate of SN nodes can reach very high values around 600 Hz [50]. Thus, for high rate of SN firing, reliable transmission of motor commands to muscles is not possible because channel capacity C_2 tends to zero.

3.6.3 Rate of Motor Information Flow to Biceps Muscle

In this part, we investigate the rate across the cascaded channels which is illustrated in Fig. 3.2 by using realistic neuron counts in a limb for a particular muscle called biceps muscle as given in Table 3.4. In this setting, SNs are assumed to be spiking

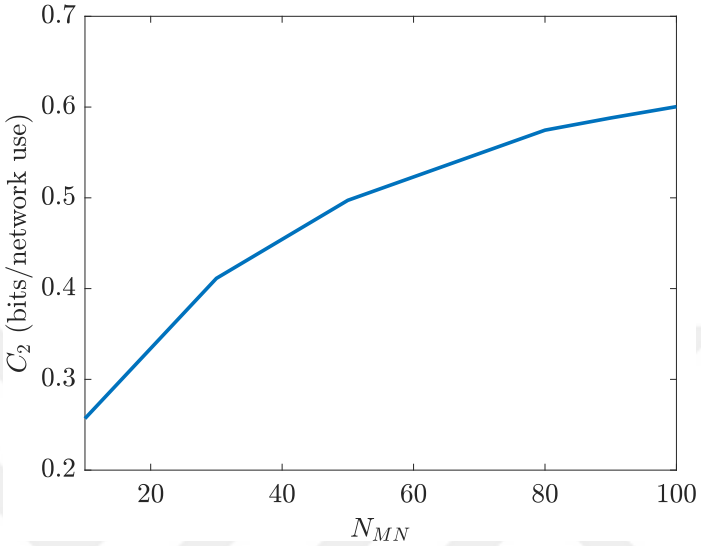

(a) $N_{ExIN} = 400$, $\lambda_{IaIN} = 80$ Hz

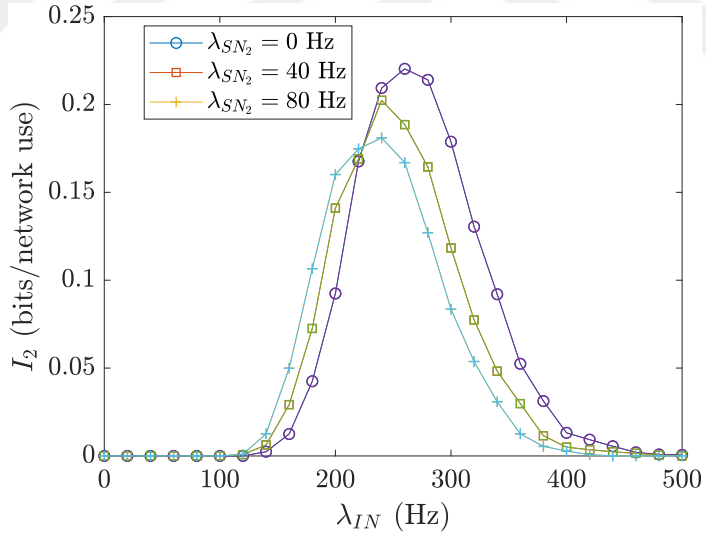

(b) $N_{MN} = 5$, $N_{ExIN} = 350$, $\lambda_{IaIN} = 90$ Hz

Figure 3.5: When $P_{rel}^{IN} = 0.8$ and $P_{rel}^{SN_2} = 0.1$, (a) Capacity of second layer for increasing number of MNs (b) Mutual information I_2 for various sensory interference levels

at average rate of 10 Hz [2] and inhibitory IN nodes (IaIN) fires at average rate of 80 Hz. Since we lack of data for N_{CN} and N_{ExIN}, enough number of neurons is used so that at least some part of post-synaptic neurons can generate spike.

As Fig. 3.6 shows, maximums of mutual informations I_1 and I_2 are comparable for biceps muscle. Hence, in case of reduction in the individual channel capacities

Table 3.4: Number of Neurons (Biceps Muscle) [2]

Class of Neuron	**EXC/INH**	**Quantity**
SN_1 (Ia-Antagonist)	EXC	~ 500
SN_2 (Ia afferent)	EXC	~ 300
IN (IaIN)	INH	~ 300
IN (ExIN)	EXC	-
MN (Alpha)	-	~ 700
CN	EXC	-

due to a damage to the particular type of neurons can result in reduction in overall network capacity because the bottleneck limits the capacity of independent cascaded channels as given by (3.1).

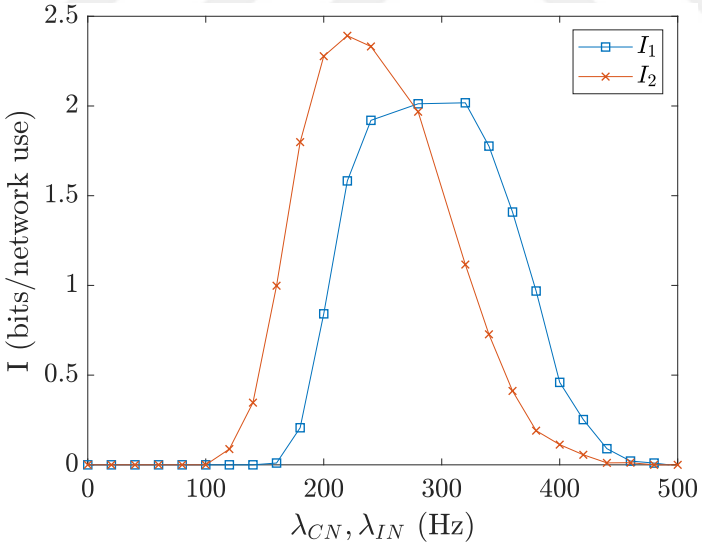

Figure 3.6: Mutual informations when $\lambda_{IaIN} = 80$ Hz,$\lambda_{SN_1} = 10$ Hz,$\lambda_{SN_2} = 10$ Hz, $N_{ExIN} = 700$, $N_{CN} = 600$.

3.7 Information Theoretical Metrics and Spinal Cord Injuries

In this section, based on our previous analysis, we reach to several results for the relation between spinal cord injuries and information theoretical metrics such as mutual information and capacity. Deduced relationship between change in mutual informa-

tion or capacity and injury symptoms can provide deeper understanding for spinal cord injuries from ICT perspective and may be used in future ICT-based diagnosis and treatment tools for neural injuries.

Upper Motor Neuron Syndrome

As aforementioned in Section 3.2, motor commands from the motor cortex are conveyed to the spinal cord through descending pathways. Upper motor neuron syndrome (UMNS) refers to the condition in which several symptoms are observed subsequent to damage to these pathways due to a disease such as multiple sclerosis (MS) or a lesion caused by brain stroke or spinal cord injury. The symptoms include weakness in movements and exaggerated reflexes. Based on our analysis, we can deduce following relations between information theoretical metrics and signs of UMNS.

- In UMNS, due to loss in CN population, capacity of brain to spinal cord channel is expected to decrease considering Fig. 3.4a. Therefore, we deduce that decrease in capacity C_1 makes the first layer bottleneck so that it results in weakness in movements because MN and IN nodes remain intact. If all CNs are damaged, then paralysis (no movement) occurs. Thus, paralysis arises from the observation that channel capacity tends to zero. On the other hand, if there is high redundancy, which means high number of CNs project to INs, then decrease in the capacity is slight as shown in 3.4a. This can be explained with the fact that other cortical neurons can compensate loss of neurons by increasing redundancy (such as increasing functional contacts) to some extent so that recovery can be achieved if the damage is slight [51].

- Since IN and MN nodes remains intact, we expect bound on the sum rate of second layer, which can be found by (3.10), remains same. However, rate of motor information flow, which expressed in (3.1), can be limited by second layer due to increased sensory interference. Loss of CNs makes SNs to fire at very high levels due to loss of some inhibitory mechanism [51]. This results in

exaggerated reflexes. As the sensory interference increases, the rate of motor information flow decreases as shown in Fig. 3.5b. At high SN firing rates λ_{SN_2}'s, I_2 can even tend to zero. Therefore, second layer can also limit the rate of motor information flow due to high rate of SN firing.

Lower Motor Neuron Syndrome

Lower Motor Neuron Syndrome (LMNS) refers to the symptoms that are result of damage to MNs, due to a disease such as Amyotrophic lateral sclerosis (ALS) or injury. Well known signs of LMNS are muscle atrophy and weakness [51]. Due to loss of MNs in a MN pool, associated muscle wastes away or being atrophied. As depicted in Fig. 3.5a, capacity of interneuron-motoneuron channel decreases with decreasing number of MN nodes. This result shows that there is a correlation between decrease in capacity and occurrence of muscle atrophy. Moreover, we can deduce that weakness in the muscle due to loss of MNs occurs when channel capacity tends to zero with the decreasing number of MN nodes. The capacity of the spinal network also tends to zero with the complete loss of MNs, since the second layer becomes bottleneck.

Chapter 4

NOVEL ICT-BASED TREATMENTS FOR SPINAL CORD INJURIES

4.1 Introduction

Fine motor movement and sensation in the human body are maintained by wired communication between the brain and the spinal cord via neural pathways. Spinal cord injuries (SCI), however, damage these pathways and healthy communication cannot be reestablished naturally. As a result, chance of recovery almost does not exists and many people with SCI experience motor and sensory deficits throughout their lives [52]. In spite of the efforts on the restoration of these pathways from medical and bio-engineering perspectives, successful treatment still does not exist. On the other hand, information and communication technology (ICT) based treatments can address intrinsic limitations of existing approaches by introducing communication and networking techniques [53].

Huge efforts have been focused on the restoration of disrupted communication between the brain and the spinal cord from medical and engineering perspectives. Complete functional recovery by medical interventions, however, is not achieved up to date. Therefore, engineering treatment approaches are proposed from bio-engineering perspective. Current bio-engineering approaches focus on employing engineered nanoagents which are capable of making therapeutic intervention in the body or designing neural interfaces bridging injured spinal cord via engineered bio-compatible materials. The idea behind these methods is reversing toxic biological response in the spinal tissue and making the injured tissue suitable for spared nerves to regrow. However, these methods have also achieved limited functional outcome [54–63]. We refer medical and

bio-engineering methods as biological methods in the following parts.

In this chapter, we focus on ICT-based treatment techniques, which can provide successful outcome by utilizing highly evolved communication and networking techniques developed to the date. ICT-based techniques for SCI treatment can be listed as, (i) employing of neural interface systems (NIS) (ii) deploying replacement artificial neurons (ANs) inside the body. In addition to operate robotic prosthesis, NIS were used to electrically stimulate the nervous system or muscles in order to restore motor function [64–67]. However, the recovery is partial [68, 69]. The idea that using engineered neurons as replacement to injured neurons, on the other hand, is a direction which is recently established. Therefore, ANs operating functionally still do not exist.

In this chapter, we present treatment techniques for SCI in the literature which include biological, NIS and AN-based approaches. The rest of this chapter is organized as follows. In Section 4.2, we give an overview for SCI and some key treatment approaches. In Section 4.3, existing ICT-based treatment techniques for SCI are described. Section 4.4 describes our proposed methods in detail. Section 4.5 states future research directions and applications.

4.2 Overview

In this section, we describe phases of injury and their affects on the nervous network, existing biological treatment techniques for SCI, and discuss the advantages of ICT-based treatments over biological treatment techniques.

4.2.1 Spinal Cord Injury Mechanisms

Neurons effected by spinal trauma experience the effects of an injury in three consecutive phases, namely, primary, secondary and chronic injury described below.

- *Primary injury:* The primary injury immediately disrupts axonal pathways and damages cell membranes depending on the physical trauma [70]. Many active neural connections are severed and neuro-spike communication is effected by the extracellular toxicity.

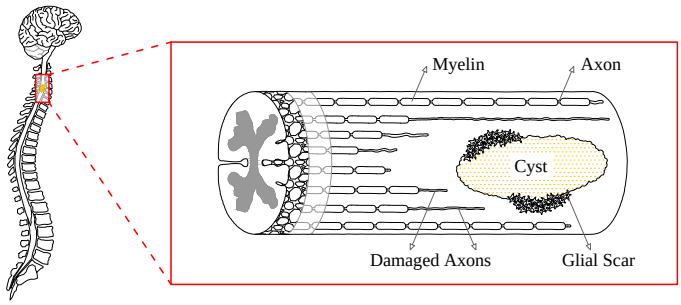

Figure 4.1: SCI and the formation of glial scars.

- *Secondary injury:* It constitutes the time interval within hours to weeks after the injury [71]. Due to toxic environment of the spinal cord supportive cells (oligodendrocytes) die [72]. Deaths of these cells cause demyelination, which is the loss of myelin insulator that surrounds axons, thereby, effecting the signal quality of the neuro-spike communications [73]. Distorting or blocking axonal propagation, demyelination eventually disconnects (partly or wholly) the brain from the spinal cord [73]. This channel outage manifests itself in sensory and motor deficits. Moreover, the formation of scar, which is a tissue that barriers axonal regeneration as shown in Fig.4.1, also occurs.

- *Chronic injury:* This phase covers the days to years following the injury [71]. In this phase, injured axons experience a special kind of degeneration, called Wallerian degeneration, that disconnects the distal parts of the axons from their cell bodies while the glial scar continues to grow [74]. Since the injury area and the neuro-spike communication occuring within it is stabilized in the chronic phase, most treatment techniques target this particular phase.

The overall result of SCI mechanisms is disruption of axonal pathways located within spinal cord, which results in either the loss of sensory information transmission to the brain or motor control signals to the muscles or both at the same time [70]. Hence, re-establishing communication system across the brain-spinal cord connection is necessary to maintain sensory and motor function of the nervous nanonetwork. As

discussed earlier, current treatment approaches fall in two main categories, namely, the biological and the ICT-based treatment techniques. In the following, we discuss the major techniques that fall under these categories and the key differences between the approaches.

4.2.2 Biological Treatment Techniques

Following the initial disruption of SCI, damage continues to spread in the spinal cord in the secondary and the chronic phases. Biological treatment approaches aims to protect surviving neurons from the toxic post-injury environment, and to recover synaptic connections and healthy functionality by promoting regeneration. On the contrary, ICT-based treatment approaches directly address the neural communication problem by either bypassing the injury site via external communication interfaces or by replacing the injured neurons by artificially designed neurons.

In the following, we outline fundamental biological treatment approaches and the challenges faced regarding their implementation. Moreover, we discuss how these challenges can be addressed by ICT-based treatment techniques.

Research efforts regarding biological treatments mainly focus on the following directions.

Neuroprotection

Delivering drugs onto the injury site is a possible method of neuroprotection. Recent research in this area concentrates on drug delivery mediated by nanomaterials such as nanowires, nanoparticles and carbon nanofibers, which have several advantages over conventional drug delivery methods such as providing targeted delivery and reaching injury site by crossing the blood-spinal cord barrier [75]. The challenges in this direction include the following.

- *Application:* Devastating effects of secondary injury mechanisms spread fast with the cascade of biological complex events. Preventing this spread means intervening many biological processes in the spinal cord with presumably number

of different neuroprotective agents. Thus, identifying the effective drugs and their administrations in a limited time period poses challenges. Moreover, there are lots of issues regarding drug carrier design are to be overcome [75].

- *Validation:* Several drugs are tested on animals and *in vitro* environments for different injury scenarios. Identifying effective drugs and methods among many alternatives and verifying the efficacy by human trials still pose a challenge.

- *Functional outcome:* Although several neuroprotective drugs are reported to be resulting in some functional recovery [76], functional outcome is limited because complete recovery also necessitates the reformation of spinal cord circuitry.

Neural regeneration

Delivery of neuro-regenerative drugs, cell-based therapy and tissue engineering aim to promote neural regeneration. In drug delivery, growth factors such as neurotrophins help in improvement of nerve regeneration, synaptic transmission and plasticity [77]. Cell therapy efforts mostly focus on cell transplantation and grafting. Transplantation of stem cells is widely investigated as a cell-based therapy [78–80], as stem cells have differentiation capabilities that allow them to change into neurons and glia. In addition, a variety of cells are used in studies such as Schwann cells that are in-charge of producing myelin sheaths in peripheral nervous system and capable of improving remyelination as well as axonal regrowth [81,82]. Tissue engineering aims to promote regeneration of injured nerves by means of materials that can mimic natural scaffolding such as hydrogels, nanofiber scaffolds and hybrid applications. Hydrogels are biocompatible networks of polymers that can improve the environment for neural regrowth [58–60]. Nanofiber scaffolds not only provide supportive scaffolding for damaged cells but also deliver drugs and support transplanted cells [55–57]. Various combinations of hydrogels, nanofibers and drugs are also studied for recovery of SCI as shown by [61–63]. Fundamental challenges in this direction include the following.

- *Functional outcome:* Although above-mentioned studies report some improvement regarding neural regeneration and recent research show several initial results regarding functional neural network formation [83–86], directing regenerating neurons to form functional circuitry still poses huge challenge in this research direction [54].

- *Human Trials:* Safety and efficacy of medicine treatment and cell therapy on humans are still controversial [54,87]. Regarding tissue engineering, functionally integrating biocompatible materials to the tissues and the feasibility of human trials are the unknown issues [88].

4.2.3 Biological versus ICT-based Treatments

Since ICT-based treatment approaches do not have protective or supportive aims, they directly focus on communication problems between the brain and the spinal cord. Several initial studies have provided promising results for these techniques with regard to safety and the functional outcome. In this respect, some advantages over biological treatment approaches are stated below.

- *Functional outcome:* As processing, stimulation and communication capabilities of the external interfaces advance with the developments in ICT, restoration in the movements of a subject with SCI can be observed as shown by a recent study [66].

- *Human trials:* In addition to animal experiments, in studies such as [67], promising improvements in terms of motor impairment in human patients were observed.

- *Safety:* Although long term safety of the invasive recording devices in NISs is still not proven, there are less invasive alternatives with low risk neural interfaces such EEG-based [89] and ECoG-based systems.

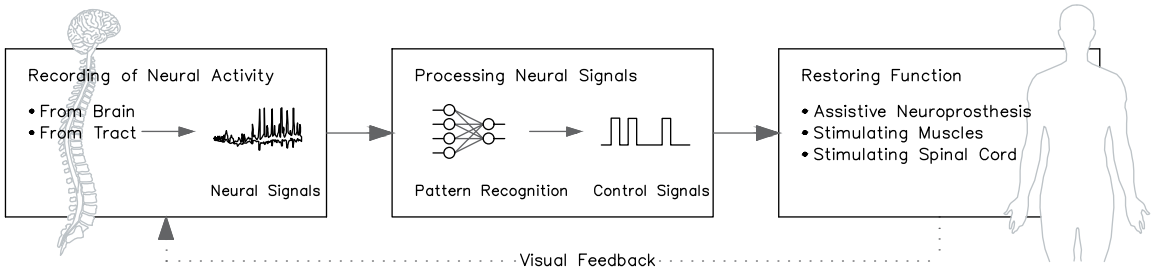

Figure 4.2: Basic structure of an NIS.

4.3 Existing ICT-based Treatment Techniques

In this section, we present prevalent ICT-based treatment techniques reported in the literature and future directions that may be possible in the NIS and AN frameworks. The two techniques contrast with each other on the scale of their approaches with NIS focusing on macro-scale solutions and AN employing a micro/nano-scale approach.

4.3.1 Neural Interface Systems

While aforementioned biological techniques aim to improve signal transmission problem through the injured spinal cord, NISs utilize nervous signals taken directly from the brain or spinal cord before the injured part to restore the motor function. The major components of a typical NIS are depicted in Fig. 4.2. Details for each of these components is given below.

Neuron Recordings

Available neuron recording methods include recording directly from the brain [66, 69, 90, 91] and recording from the spinal cord tracts [92]. Efficacy, safety, reliability and longevity are the important factors regarding neuron recordings. In the following, we discuss neuron recording methods.

Brain Recordings In contrast to non-invasive recoding techniques, recordings with exceptionally high SNR and high spatio-temporal resolution can be achieved by in-

vasive recording techniques such as electrocorticography (ECoG) and intracortically electrode placements [93]. In ECoG, electrodes are implanted subdurally on the surface of the brain, hence, they are able to record the activity of groups of neurons and provide movement-related field potentials. These recordings are robust over long periods [94] and higher spatial resolutions can be achieved by utilizing micro-ECoG grids [95]. Moreover, [96, 97] demonstrates that it can provide enough independent control signals for simple loco-motor task.

Recording from Spinal Cord Tracts Recording motor control signals through cross sectional area of corticospinal tract is investigated in [92,98] to obtain recordings with higher precision than the brain recordings. Main drawbacks of this method are given as follows.

- Designing a mechanically stable array of electrodes is challenging.
- The range of signal capture by an electrode array is limited, and thus, the number of neural sources are far more than the array recording electrode contacts.
- Lack of control signals obtained from the tracts for patients with complete SCI or ALS.

Signal Processing

Real-time processing of the recorded neural data needs to be done for deriving the intended task by the patient. This process is seen as a pattern recognition system that contains three main parts: (i) feature extraction, (ii) dimension reduction and feature selection, (iii) classification or regression. First, the data is processed to derive a set of features. Feature sets extract the discriminating information that represent a dataset. Dimension reduction and feature selection methods are utilized to remove irrelevant and redundant information. In Table 4.1, a list of methods available for each step of a pattern recognition system is provided [99].

Table 4.1: A list of methods used in a pattern recognition system.

Process	**Method**
Feature extraction	AutoRegressive component
	Wavelet transform
	Common spatial pattern
	Matched filtering
Dimension reduction	Principal component analysis
	Independent component analysis
Feature selection	Genetic algorithm
	Sequential selection
Classification	Linear discriminant analysis
	Support vector machine
	Bayesian statistical classifier
	K-nearest neighbor classifier
	Artificial neural network

After extracting the intended task from neural recordings, control signals must be derived to restore or replace natural function of a paralyzed or lost limb. In case of spinal cord stimulations for restoring the functionality of the injured spinal cord, these control signals are the parameters needed as the input of the spinal cord stimulator.

Restoration of Function

The extracted control signals from the previous steps are then utilized to restore or replace natural function of a paralyzed or lost limb. Such NISs include brain-computer/machine/spine interfaces [64–67, 69, 90, 99–110], or spinal cord-computer interfaces [92, 98] that are further described below.

Operating assistive neuroprosthesis Using assistive neuroprosthesis is not the focus of this study since it does not provide a solution for bypassing the injured part of the spinal cord to restore the control over muscles.

Direct stimulation of muscles Direct stimulation of muscles by signals extracted from intracortically recordings was first studied on monkeys with transiently paralyzed

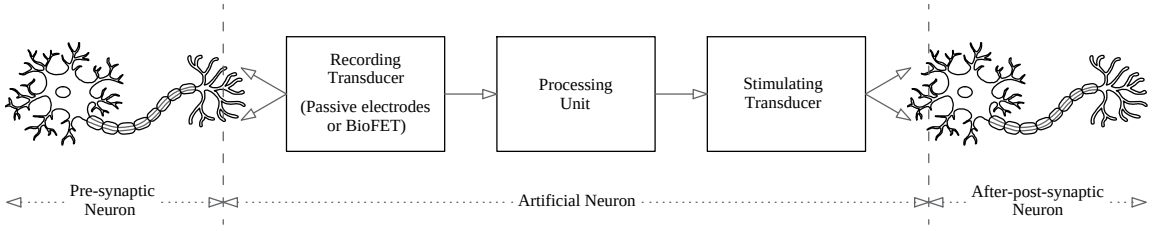

Figure 4.3: The general architecture of an artificial neuron.

arm [64, 109, 110], and then applied to a paralyzed human [67]. Results suggest that intracortical recordings can be linked in real-time to muscle activation, enabling the control of muscles using the activity of neurons in the motor cortex. However, electrical stimulation of muscles causes fatigue and long term stimulation by electrodes can damage muscles.

Spinal cord stimulation Epidural spinal cord stimulation and intraspinal microstimulation are two existing methods in the literature for inserting motor control signals back to the motor circuitries. However, by using current electrical stimulation techniques in either epidural stimulation or intraspinal microstimulation, cell specific activation of spinal cord's motor circuitry is challenging due to interference from non-target neuron populations. In this respect, optogenetics can be a key to control the limbs by activating or suppressing specific population of neurons in the spinal cord [111, 112]. Open issues include finding encoding methods for motor commands recorded from the brain in order to deliver meaningful signals to the spinal cord and developing proper light delivery techniques for spinal cord [113]. The former requires identifying contributions of different neuron populations on the motor control. Regarding the latter, current research focuses on RF powered wireless systems [114,115] since employing optical fibers in the spinal cord is not possible contrary to the case of brain [113]. Another approach could be designing ultrasound powered optogenetic stimulator systems such as shown in [116, 117], which can reach deeper layers in the spinal cord, to employ them in the spinal cord.

4.3.2 Artificial Neurons

Another potential direction for treatment of SCI could be the use of artificially created neurons to replace injured biological neurons. The general architecture of an AN is shown in Fig. 4.3, where a pre-synaptic neuron connects to a processing unit by means of a transducer. The AN performs processing actions similar to its biological counterparts, and thus, completes the nervous pathways. Some key characteristics required by a functioning AN that may replace biological neurons are outlined below.

- *Plasticity:* The AN should be able to change synaptic weights in a plastic manner since plasticity forms the basis of memory and cognitive functions of the nervous system.

- *Implementation scale:* From the perspective of a single neuron, the scale can either be synaptic or neuronal. On synaptic scale, individual synapses can be identified and interfaced to synapses from other neurons, whereas on neuronal scale, the neuron as a whole may be interfaced.

- *Biocompatibility:* The AN should be bio-compatible such that this bio-compatibility should extend to the bio-interfaces of an AN within the body [118].

- *Physical dimension:* The sizes of the AN should be on a scale similar to biological neurons. Synaptic clefts are on average 20 nm in length, whereas spinal neurons are significantly larger in size.

- *Energy requirements:* Energy self-reliance is another major issue for any implanted system. Batteries may not be a viable solution for long term implantation. The energy required by an AN can be harvested from the body heat or blood pressure by creating gradients within the body.

- *Amplification:* Processing of biological inputs may require with low noise, low power and high precision characteristics.

- *Implantation:* This process is almost as critical as the development of ANs themselves. On scales of neurons, surgery by human surgeons is not a viable solution. In such cases, robotic surgery system would need to automatically identify different sections of biological neuron by means of imaging, and proceed with the surgery by connecting the appropriate AN sections accordingly.

The characteristics of the AN discussed above provide significant challenges; however, once developed, the benefits of such systems are also unlimited.

4.4 Proposed ICT-based Treatment Techniques

In this section, we introduce critical enhancements of two potential techniques for SCI treatment based on the literature survey and the desired characteristics of NIS and AN.

4.4.1 Neural Interface Systems with Sensory Feedback

The main technical challenges in using an NIS to provide an ICT-based treatment for spinal cord injuries can be itemized as follows.

- *Restoring Somatosensory Feedback*: Current NISs are unidirectional which is meaning that motor commands from the brain are decoded and delivered to actual or prosthetic limbs. Natural sensory feedback to the system is provided by visual feedback only. On the other hand, by unidirectional approach, fine motor actions cannot be restored because only vision does not provide complete sensory feedback from the body. It is shown that with visual feedback only, movements are slow and uncoordinated [119]. Hence, encoding feedback from multiple sensory modalities such as touch and proprioception and deliver them to the brain [120] can improve fine movements.

- *Recording and Stimulation Techniques*: Graphene is a novel bio-compatible 2d-material and its sensitivity to different ions can be modified by various etching

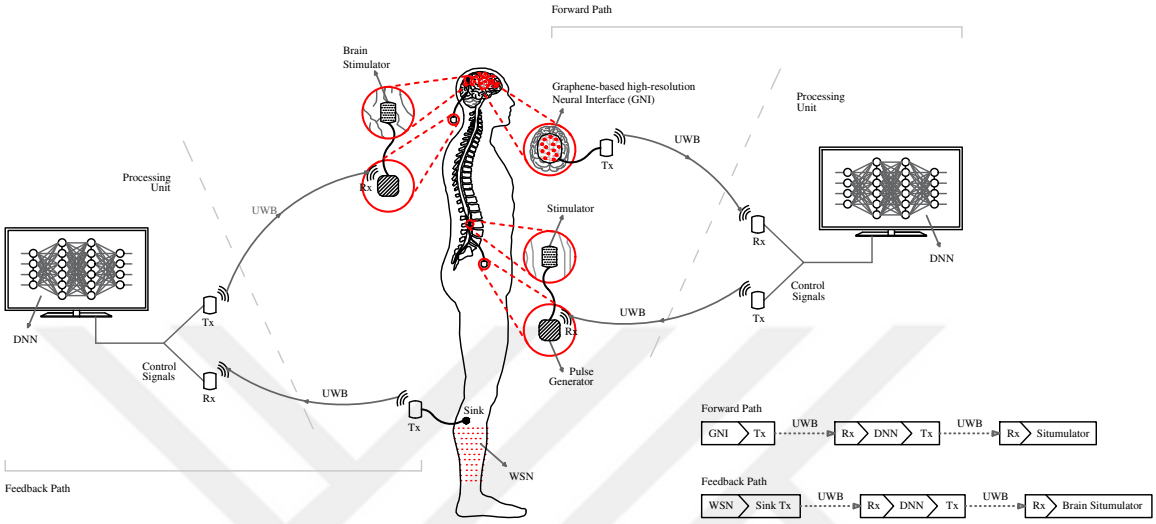

Figure 4.4: Proposed NIS system with enhanced feedback.

methods and functionalization [121]. Hence, it can be used for sensing fluctuations in specific ion concentrations. Graphene is electrically conductive, and it can be patterned into nanoscale, electrically disconnected, conductive patches via hydrogenation, etching or fluorination [122, 123]. This makes it suitable for implementing high resolution neural interfaces which can both generate and differentiate the highly localized fluctuations in ion concentrations.

- *Fully Implantable System*: To offer more comfort for patients and reduces the risk of inflammation, the NIS must be fully implantable.

In this section, we propose the comprehensive framework for realizing an NIS that addresses the above mentioned challenges. Our proposed NIS that utilizes the neural signals recorded from the brain and stimulates the spinal cord for restoring motor function in paralyzed patients is shown in Fig. 4.4. Different components of our NIS are explained in the following.

Recording Device and Processing Unit Communication Interface

The graphene-based high resolution neural interface (GNI) will be placed over the primary motor cortex to record the brain activities of the patient. This recording

device is implanted together with a transmitter, which uses wireless transmission to communicate recorded signals with a processing unit.

The bandwidth demand of the wireless transmission channel between the brain implant and the external processing unit is correlated with the number of recording channels employed. For better estimation of brain commands, we need densely distributed recording sites that require high data rates (on the order of Mbps) [124]. On the other hand, the transmitter should dissipate relatively low energy because thermal heat produced by power consumption can damage neural tissues [125]. Considering these limitations, Ultra-wide band (UWB: 3.1-10.6 GHz) systems, which can provide high data rate within allowable power dissipation range with minimal chip area [126], is the most suitable solution [127]. Therefore, the communication interface between the brain implant-processing unit of our NIS will consist of a simple UWB transmitter at the brain implant and a more complex UWB receiver at the processing unit [128]. Furthermore, compression techniques with efficient implementation, such as the one proposed in [129] can be utilized to reduce data rate without considerably affecting complexity.

Processing Unit and Spinal Cord Stimulator Interface

The processing unit performs two tasks, (i) decoding the intent of the subject from neural signals, and (ii) generating control signals for spinal cord stimulation. This unit will be placed in a rechargeable and mobile device. Hence, it needs a wireless transmitter to transfer the stimulation parameters to the site of spinal cord stimulation. The transmission between the processing unit and spinal cord neural stimulator can be performed at lower data rates compared to the brain implant-to-processing unit link since the dimensionality of the transmitted signal reduces. Additionally, the receiver at the neural stimulator must operate with low energy [125]. Transmission at low signal energy and minimal antenna coverage area again makes UWB transmission suitable for this link. Moreover, it is also advantageous in terms of interference [130].

The received control signals at the spinal cord stimulator are then used for setting the stimulation parameters. The GNI is able to both recognize and generate fluctuations in concentration of specific molecules in a local area. Hence, it will also be used for high resolution stimulating of nerve cells located in spinal cord.

Muscle to Brain Communication Interface (Feedback)

There are variety of wearable sensor for monitoring body activity in the literature. Among these, especially flexible tattoo-based and skin-like sensors are advantages due to their soft and ultra thin designs that provide comfort for users. Moreover, they are generally made of bicompatible materials such as graphene [131–134] and gold [135], which makes them suitable for long term use. These sensors are also capable of recording multiple sensory modalities such as muscle activity and touch [131]. Considering communication interface, wired, wireless or hybrid approaches can be followed. For high density of sensors, which is the case of multiple modalities being recorded, we can use wired sensor arrays whose recordings are gathered at the sink node, which has wireless communication interface with the processing unit or with the brain implant directly. Otherwise, communication modules of the sensors can be integrated to Near Field Communication (NFC) and Radio Frequency Identification (RFID) technologies, which are enabled by flexible thin antennas such as graphene-based antenna shown in [136].

An alternative to wearable sensors is ultrasound-based implantable Neural dust, which is validated in rat peripheral nerves and is shown to be capable of recording neural activity in the peripheral nervous system [137]. This system uses backscattering and other advantageous aspects of ultrasound such low attenuation through the tissues, and accordingly low energy consumption compared to RF technologies currently employed in implantable devices [138]. In addition to this, further miniaturization is needed in this system as well as in the aforementioned flexible sensor based systems.

The collected sensory information is then transmitted to the processing unit to

generate the parameters for somatosensory cortex stimulation. For this aim, the responsible regions of somatosensory cortex for sensory feedback from each leg should be identified as follows. The placements of stimulation electrodes on the brain and sensors on the body require mapping between the outputs from each sensor and location in S1. Somatotopic organization of S1 [139], which is one to one correspondence between a sensation from a body part and population of neurons in S1, enables such mapping. To this aim, the subject is trained (no need for training in the case of human subject [140]) by stimulating 3a and 3b areas of S1, which are related to proprioception and touch [141]. According to the report of subject, the perceived locations on the limbs are determined. The sensors that will provide the feedback then will be placed on these locations. For the paralyzed subjects, the mapping is performed using remaining sensory connections; however, in the case of complete sensory loss, new techniques are required. Afterwards, a DNN is trained to estimate the activity of somatosensory cortex according to the collected sensory information. Since we consider the SCI injuries in which the sensory pathway is also damaged, our NIS will utilize this information to generate stimulation parameters that activate similar somatosensory regions in patients.

In the next step, the processing unit transmits the stimulation parameters to the controller unit that is surgically placed over pia mater. The transmission will be performed through UWB communication interface again. The controller sends the control signals to the graphene based high resolution neural interface located over somatosensory region to stimulate the brain through manipulating ionic concentration levels.

4.4.2 Self-Organizing Artificial Neurons

Although the nervous system's information processing capacity increases by the use of an NIS, its capacity is not as high as before the injury due to unrecoverable information loss. A solution to the aforementioned problem could be the retrieval of connections lost at the injury cite. The capacity could be maximized (at least theoret-

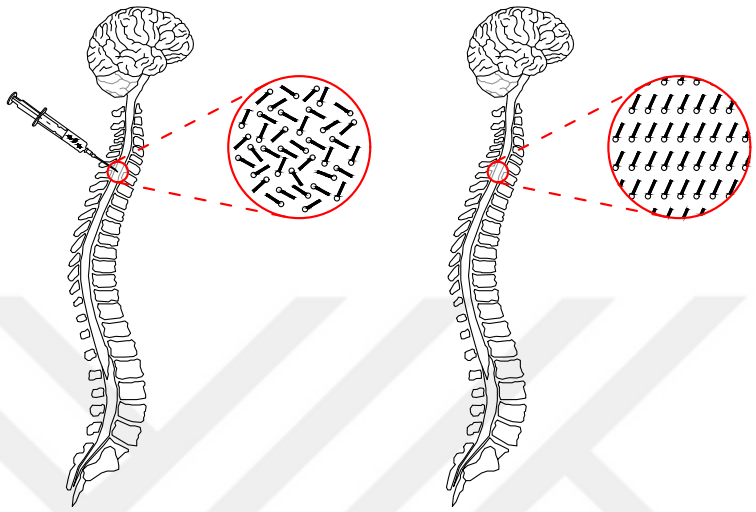

(a) Before self-organization. (b) After self-organization.

Figure 4.5: Self-organizing ANs incorporated into hydrogel.

ically) to the pre-injury levels by employing artificial nervous connections across the injury area where the signals are already localized in specific positions. Therefore, we propose an architecture where ANs with neuromorphic properties are suspended in a hydrogel. Such ANs, can form bridges across the injury cite and make new nervous connections with biological and artificial neurons. A representative diagram is shown in Fig. 4.5.

As discussed earlier, the implantation of AN systems propose a major challenge since surgery on the micro/nano-scale itself is an open problem. This problem can be bypassed by considering systems that use self-organization to create the AN bridge across the nervous injury. Such a system is shown in Fig. 4.5, where AN bridges form across the injury area over time. Self-organization is a hot research area, where local interactions between individual entities give rise to an overall structure of the system. The simplest approach towards this goal is the use of electric or magnetic fields. Since the action potentials of the nervous system are themselves electrical signals, the self-organization can be based on its use as the attractor field. Graphene nanosolenoids discussed in [142] may provide the ideal implements in this regard both in terms the

required size, low energy requirements and magnetic properties.

For the system to be completely independent, the ANs need to collect energy from their environment. This energy can be scavenged within the body [143], or through external sources using wireless power transfer (WPT).

4.5 Applications of ICT-based SCI treatment techniques

ICT-based treatments for SCI can also open the way for number of applications in different scenarios. Internet of Bio-Nano Things (IoBNT) framework [4] is a basis for applications in which biological entities will be connected to Internet. Regarding the deployment of engineered nano entities in the body, wide range of applications including remote health monitoring and smart delivery systems can be envisioned. In case of NIS, interfacing brain with the Internet can maintain direct interaction between the brain and the living/inanimate things so that applications such as smart home, smart city and smart hospital can be enabled. In the following, we describe some examples of these applications.

Regarding the former, in a targeted drug delivery scenario, the patient can receive different drug and enzyme treatments. Therapeutic intervention of SCI, especially neural regeneration, is a long process which may take weeks or years. Therefore, This shows the need for remote monitoring and treatment. In such a case, successful delivery signal of a particular type of therapeutic molecules can be received by a bio-cyber interface, which can be positioned near the spinal cord column according to the site of injury, and then be transmitted to medical personnel through the Internet. According to health condition of the patient, the medical personnel can decide to use another treatment and send a activation signal to the bio-cyber interface. The bio-cyber interface transmits a signal to a particular nanosytem in order to activate it. Another IoBNT application can be remote monitoring of the patient to observe functional outcome of the treatment. In this scenario, a nanosystem monitors the activity of neurons that are original synaptic targets of the injured neurons. For instance, the nanosystem can sense neurotransmitters concentration released from

these target neurons to monitor the synaptic activity. If there is activity, this means that some of the injured neurons have reached their targets by axonal regeneration. To monitor whether the synaptic activity results in functional outcome such as motor action in the muscle as well, another nanosystem can monitor neural activity of a muscle fiber. Both nanosystems send information through the bio-cyber interface and the medical personnel can observe status of the treatment on the Internet and accordingly he or she may take actions such as activating another treatment options by sending new commands to the bio-cyber interface.

Considering NIS, recorded command signals from the brain such as ECoG signals are sent to cloud server through the Internet. Decoding of brain signals are performed in the cloud using deep learning model of the person. Decoded signal can trigger a function in intended applications.

Chapter 5

CONCLUSION AND FUTURE RESEARCH DIRECTIONS

Enabling technologies including nanotechnology have been opened the way for nanoscale bio-inspired communication systems and ICT-based treatment techniques for neural diseases. In this respect, framework for developing ICT-based diagnosis and treatment techniques was introduced in [5]. According to the framework, the development of these techniques requires the understanding of healthy and diseased intra-body communication channels as a first step and further ICT-based analysis is needed to extract the relationship between nervous diseases and network metrics. Thus, in this thesis, we focused on the modeling and information theoretical analysis of spinal cord networks and based on our analysis we reached results regarding information theoretical metrics and SCI. Moreover, we put forth novel ICT-based treatments for the treatment of SCI and reveal their future applications. The contributions and the results reached in each chapter are summarized as follows.

5.0.1 Information Theoretical Analysis of Multi-terminal Neuro-spike Networks in Spinal Cord

Extensive research effort has focused on the modeling and analysis of neuro-spike communication and other conceptual communication models for neural communication. However, a realistic communication network abstraction of spinal cord system taking physiological characteristics of neurons into account is not considered in the literature. Thus, in this chapter, we analyze rate of information flow across a spinal cord motor nucleus system from information theoretical perspective. To this end, we first develop an equivalent single-hop neuro-spike network and then formulate bound on the total achievable rates across the network. Finally, we simulate maximum achievable rates

numerically with regard to a particular spinal cord motor nucleus system. The results indicate a correlation between decreasing maximum total rates and weakness in the muscle as a result of lower motor injury.

5.0.2 Rate of Information Flow Across Layered Neuro-spike Networks in Spinal Cord

Neuro-spike communication is one of the bio-compatible communication techniques proposed to be employed among replacement nano-entities to recover the disrupted spinal cord network after SCI. Most studies regarding neuro-spike communication have been focused on realistic modeling and analysis of physical channels. In these studies, neurons are generally assumed to be cortical neurons. On the other, communication among distinct populations of neurons in the spinal cord network is not considered. Therefore, in this chapter, we model the spinal cord motor pathway as layered neuro-spike communication network in order to determine the rate of motor information flow across the spinal cord. Since the corresponding network is cascade of two independent X-channel, the network capacity is limited by minimum hop capacity. Thus, we formulate the capacity expression for neuro-spike X-channel and further derive the upper bound on the capacity for full excitatory synaptic connections. Based on our analysis on the network by using realistic data for channel and network parameters, we reach the following results. Paralysis due to loss of CNs is observed because the network capacity tends to zero as the number of CNs moves to zero. Furthermore, reduction in the channel capacity due to MN loss is correlated with occurrences of muscle atrophy and weakness which are observed in LMNS.

5.0.3 Novel ICT-based Treatments for Spinal Cord Injuries

Huge research effort has been focused on developing techniques to restore motor actions and sensation after SCI by medical and bio-engineering approaches such as drug delivery. However, successful treatment methods still does not exist because of intrinsic limitations of these approaches. On the other hand, ICT-treatment techniques can pave the way for smarter restoration of spinal cord communication pathways

by advanced communication and networking methods. Therefore, in this chapter, we propose two ICT-based treatments, namely, NIS with enhanced sensory feedback restoring both sensory and motor deficits and intra-body deployment of ANs replacing injured neurons. NIS with enhanced feedback can result in fine motor movements with the restoration of spinal sensory pathways. For ANs, we propose the use of self-organization to smartly tackle transplant issues and energy harvesting to make the devices truly independent. Moreover, development of these methods can enable IoBNT applications such as remote health-care monitoring. Furthermore, the brain can be interacted with livings and things using recorded brain signals and through bio-cyber interfaces.

5.1 Future Research Directions

In this thesis, we consider several injury scenarios affecting healthy information flow across the spinal cord. In order to reveal the relationship between information theoretical metrics and injuries, we simulated SCI with the loss of upper or lower motor neurons because the loss of these neurons affects normal functioning of the spinal cord most dominantly. However, more detailed injury scenarios using post-injury physiological data for metabolic constraints such as deficiency in energy source (ATP) of neurons and changed parameters such as release probability and post-synaptic potential amplitude can be considered as a future work. These injury models can be used in nanonetwork simulators and diagnosis tools for SCI. Moreover, neuro-spike network models can be further extended by including spinal sensory pathways as well to investigate sensory deficits due to SCI. Most importantly, experimental verifications are needed for neuro-spike communication models before prototyping replacement artificial neurons with bio-inspired capabilities which are envisioned to be employed inside the body.

BIBLIOGRAPHY

[1] R. R. Cisi and A. F. Kohn, "Simulation system of spinal cord motor nuclei and associated nerves and muscles, in a web-based architecture," *Journal of computational neuroscience*, vol. 25, no. 3, pp. 520–542, 2008.

[2] M. Sreenivasa, K. Ayusawa, and Y. Nakamura, "Modeling and identification of a realistic spiking neural network and musculoskeletal model of the human arm, and an application to the stretch reflex," *IEEE Transactions on Neural Systems and Rehabilitation Engineering*, vol. 24, no. 5, pp. 591–602, 2016.

[3] S. Kannan and P. Viswanath, "Capacity of multiple unicast in wireless networks: A polymatroidal approach," *IEEE Transactions on Information Theory*, vol. 60, no. 10, pp. 6303–6328, 2014.

[4] I. Akyildiz, M. Pierobon, S. Balasubramaniam, and Y. Koucheryavy, "The internet of bio-nano things," *IEEE Communications Magazine*, vol. 53, no. 3, pp. 32–40, 2015.

[5] O. B. Akan, H. Ramezani, T. Khan, N. A. Abbasi, and M. Kuscu, "Fundamentals of molecular information and communication science," *Proceedings of the IEEE*, vol. 105, no. 2, pp. 306–318, 2017.

[6] E. Balevi and O. B. Akan, "A physical channel model for nanoscale neuro-spike communications," *IEEE Transactions on Communications*, vol. 61, no. 3, pp. 1178–1187, 2013.

[7] D. Malak and O. B. Akan, "A communication theoretical analysis of synaptic multiple-access channel in hippocampal-cortical neurons," *IEEE Transactions on communications*, vol. 61, no. 6, pp. 2457–2467, 2013.

[8] T. Khan, B. A. Bilgin, and O. B. Akan, "Diffusion-based model for synaptic molecular communication channel," *IEEE transactions on nanobioscience*, vol. 16, no. 4, pp. 299–308, 2017.

[9] H. Ramezani and O. B. Akan, "A communication theoretical modeling of axonal propagation in hippocampal pyramidal neurons," *IEEE transactions on nanobioscience*, vol. 16, no. 4, pp. 248–256, 2017.

[10] ——, "Information capacity of vesicle release in neuro-spike communication," *IEEE Communications Letters*, vol. 22, no. 1, pp. 41–44, 2018.

[11] ——, "Synaptic channel model including effects of spike width variation," in *Proceedings of the Second Annual International Conference on Nanoscale Computing and Communication*. ACM, 2015, p. 11.

[12] H. Ramezani, C. Koca, and O. B. Akan, "Rate region analysis of multi-terminal neuronal nanoscale molecular communication channel," in *Proceedings of IEEE Nano 2017*. IEEE, 2017.

[13] N. A. Abbasi and O. B. Akan, "A queueing-theoretical delay analysis for intrabody nervous nanonetwork," *Nano Communication Networks*, vol. 6, no. 4, pp. 166–177, 2015.

[14] H. Tezcan, S. F. Oktug, and F. N. Kök, "Employing tdma protocol in neural nanonetworks in case of neuron specific faults," *IEEE transactions on nanobioscience*, vol. 14, no. 6, pp. 572–580, 2015.

[15] E. Balevi and R. D. Gitlin, "An inherent fog network: Brain-spinal cord-nerve networks," *IEEE Access*, 2018.

[16] M. Veletić, P. A. Floor, Y. Chahibi, and I. Balasingham, "On the upper bound of the information capacity in neuronal synapses," *IEEE Transactions on Communications*, vol. 64, no. 12, pp. 5025–5036, 2016.

[17] A. S. Cacciapuoti, A. Piras, and M. Caleffi, "Modeling the dynamic processing of the presynaptic terminals for intrabody nanonetworks," *IEEE Transactions on Communications*, vol. 64, no. 4, pp. 1636–1645, 2016.

[18] H. Ramezani, T. Khan, and O. B. Akan, "Sum rate of miso neuro-spike communication channel with constant spiking threshold," *IEEE Transactions on NanoBioscience*, 2018.

[19] D. Purves, G. J. Augustine, D. Fitzpatrick, L. C. Katz, A.-S. LaMantia, J. O. McNamara, and S. M. Williams, "Neuroscience. sunderland," *MA: Sinauer Associates*, 2001.

[20] M. Veletić, P. A. Floor, Z. Babić, and I. Balasingham, "Peer-to-peer communication in neuronal nano-network," *IEEE Transactions on Communications*, vol. 64, no. 3, pp. 1153–1166, 2016.

[21] V. Matveev and X.-J. Wang, "Implications of all-or-none synaptic transmission and short-term depression beyond vesicle depletion: a computational study," *Journal of Neuroscience*, vol. 20, no. 4, pp. 1575–1588, 2000.

[22] A. Zador, "Impact of synaptic unreliability on the information transmitted by spiking neurons," *Journal of Neurophysiology*, vol. 79, no. 3, pp. 1219–1229, 1998.

[23] S. REDMAN, "Quantal analysis of synaptic potentials in neurons of the central nervous system," *Physiological Reviews*, vol. 70, no. 1, pp. 165–198, 1990.

[24] A. A. Alabi and R. W. Tsien, "Synaptic vesicle pools and dynamics," *Cold Spring Harbor perspectives in biology*, vol. 4, no. 8, p. a013680, 2012.

[25] J. P. Pierce and L. M. Mendell, "Quantitative ultrastructure of ia boutons in the ventral horn: scaling and positional relationships," *Journal of Neuroscience*, vol. 13, no. 11, pp. 4748–4763, 1993.

[26] G. Buzsáki and K. Mizuseki, "The log-dynamic brain: how skewed distributions affect network operations," *Nature Reviews Neuroscience*, vol. 15, no. 4, p. 264, 2014.

[27] P. C. Petersen and R. W. Berg, "Lognormal firing rate distribution reveals prominent fluctuation–driven regime in spinal motor networks," *Elife*, vol. 5, 2016.

[28] J. Du, "Cooperative strategies in multi-terminal wireless relay networks," Ph.D. dissertation, KTH Royal Institute of Technology, 2012.

[29] T. M. Cover and J. A. Thomas, *Elements of information theory*. John Wiley & Sons, 2012.

[30] J. A. Gallego, J. L. Dideriksen, A. Holobar, J. Ibáñez, V. Glaser, J. P. Romero, J. Benito-León, J. L. Pons, E. Rocon, and D. Farina, "The phase difference between neural drives to antagonist muscles in essential tremor is associated with the relative strength of supraspinal and afferent input," *Journal of Neuroscience*, vol. 35, no. 23, pp. 8925–8937, 2015.

[31] A. Prochazka and M. Gorassini, "Models of ensemble firing of muscle spindle afferents recorded during normal locomotion in cats," *The Journal of physiology*, vol. 507, no. 1, pp. 277–291, 1998.

[32] Y. Prut and S. I. Perlmutter, "Firing properties of spinal interneurons during voluntary movement. i. state-dependent regularity of firing," *Journal of Neuroscience*, vol. 23, no. 29, pp. 9600–9610, 2003.

[33] Electrophysiological properties of spinal cord ventral horn motor neuron alphas from literature. [Online]. Available: https://neuroelectro.org/neuron/177/

[34] A. S. Finkel and S. J. Redman, "The synaptic current evoked in cat spinal motoneurones by impulses in single group 1a axons." *The Journal of Physiology*, vol. 342, no. 1, pp. 615–632, 1983.

[35] N. J. Moore, G. S. Bhumbra, J. D. Foster, and M. Beato, "Synaptic connectivity between renshaw cells and motoneurons in the recurrent inhibitory circuit of the spinal cord," *Journal of Neuroscience*, vol. 35, no. 40, pp. 13 673–13 686, 2015.

[36] M. Kuno and J. Weakly, "Quantal components of the inhibitory synaptic potential in spinal motoneurones of the cat," *The Journal of physiology*, vol. 224, no. 2, pp. 287–303, 1972.

[37] A. J. P. Fink, *Exploring a behavioral role for presynaptic inhibition at spinal sensory-motor synapses*. Columbia University, 2013.

[38] G. Stuart and S. Redman, "Voltage dependence of ia reciprocal inhibitory currents in cat spinal motoneurones." *The Journal of physiology*, vol. 420, no. 1, pp. 111–125, 1990.

[39] L. A. Elias, R. N. Watanabe, and A. F. Kohn, "Spinal mechanisms may provide a combination of intermittent and continuous control of human posture:

predictions from a biologically based neuromusculoskeletal model," *PLoS computational biology*, vol. 10, no. 11, p. e1003944, 2014.

[40] Electrophysiological properties of neocortex pyramidal cell layer 5-6s from literature:. [Online]. Available: https://neuroelectro.org/neuron/111/

[41] D. G. Stein and S. W. Hoffman, "Concepts of cns plasticity in the context of brain damage and repair," *The Journal of head trauma rehabilitation*, vol. 18, no. 4, pp. 317–341, 2003.

[42] F. J. Alvarez, K. L. Bullinger, H. E. Titus, P. Nardelli, and T. C. Cope, "Permanent reorganization of ia afferent synapses on motoneurons after peripheral nerve injuries," *Annals of the New York Academy of Sciences*, vol. 1198, no. 1, pp. 231–241, 2010.

[43] D. Malak and O. Akan, "Communication theoretical understanding of intrabody nervous nanonetworks," *IEEE Communications Magazine*, vol. 52, no. 4, pp. 129–135, 2014.

[44] R. N. Lemon, "Descending pathways in motor control," *Annu. Rev. Neurosci.*, vol. 31, pp. 195–218, 2008.

[45] M. A. Khojastepour, A. Sabharwal, and B. Aazhang, "Bounds on achievable rates for general multi-terminal networks with practical constraints," in *Information processing in sensor networks*. Springer, 2003, pp. 146–161.

[46] L. Fenton, "The sum of log-normal probability distributions in scatter transmission systems," *IRE Transactions on Communications Systems*, vol. 8, no. 1, pp. 57–67, 1960.

[47] N. B. Mehta, J. Wu, A. F. Molisch, and J. Zhang, "Approximating a sum of random variables with a lognormal," *IEEE Transactions on Wireless Communications*, vol. 6, no. 7, 2007.

[48] Neuroelectro.org. [Online]. Available: https://neuroelectro.org/neuron/1865

[49] M.-P. Cote, L. M. Murray, and M. Knikou, "Spinal control of locomotion: Individual neurons, their circuits and functions," *Frontiers in Physiology*, vol. 9, p. 784, 2018.

[50] A. Prochazka, "Proprioceptive feedback and movement regulation."

[51] 2018. [Online]. Available: https://nba.uth.tmc.edu/neuroscience/s3/chapter06.html

[52] "Spinal cord injury (sci) 2016 facts and figures at a glance," *The Journal of Spinal Cord Medicine*, vol. 39, no. 4, pp. 493–494, 2016, pMID: 27471859. [Online]. Available: http://dx.doi.org/10.1080/10790268.2016.1210925

[53] O. B. Akan, H. Ramezani, T. Khan, N. A. Abbasi, and M. Kuscu, "Fundamentals of molecular information and communication science," *Proceedings of the IEEE*, 2016.

[54] P. Assinck, G. J. Duncan, B. J. Hilton, J. R. Plemel, and W. Tetzlaff, "Cell transplantation therapy for spinal cord injury," *Nature Neuroscience*, vol. 20, no. 05, pp. 637–647, 2017.

[55] Y. Liu, H. Ye, K. Satkunendrarajah, G. S. Yao, Y. Bayon, and M. G. Fehlings, "A self-assembling peptide reduces glial scarring, attenuates post-traumatic inflammation and promotes neurological recovery following spinal cord injury," *Acta biomaterialia*, vol. 9, no. 9, pp. 8075–8088, 2013.

[56] J. Guo, H. Su, Y. Zeng, Y.-X. Liang, W. M. Wong, R. G. Ellis-Behnke, K.-F. So, and W. Wu, "Reknitting the injured spinal cord by self-assembling peptide nanofiber scaffold," *Nanomedicine: Nanotechnology, Biology and Medicine*, vol. 3, no. 4, pp. 311–321, 2007.

[57] V. M. Tysseling-Mattiace, V. Sahni, K. L. Niece, D. Birch, C. Czeisler, M. G. Fehlings, S. I. Stupp, and J. A. Kessler, "Self-assembling nanofibers inhibit glial scar formation and promote axon elongation after spinal cord injury," *Journal of Neuroscience*, vol. 28, no. 14, pp. 3814–3823, 2008.

[58] S. Kabu, Y. Gao, B. K. Kwon, and V. Labhasetwar, "Drug delivery, cell-based therapies, and tissue engineering approaches for spinal cord injury," *Journal of Controlled Release*, vol. 219, pp. 141–154, 2015.

[59] P. Krsko, T. E. McCann, T.-T. Thach, T. L. Laabs, H. M. Geller, and M. R. Libera, "Length-scale mediated adhesion and directed growth of neural cells by surface-patterned poly (ethylene glycol) hydrogels," *Biomaterials*, vol. 30, no. 5, pp. 721–729, 2009.

[60] M. J. Mahoney and K. S. Anseth, "Three-dimensional growth and function of neural tissue in degradable polyethylene glycol hydrogels," *Biomaterials*, vol. 27, no. 10, pp. 2265–2274, 2006.

[61] B. Chen, J. He, H. Yang, Q. Zhang, L. Zhang, X. Zhang, E. Xie, C. Liu, R. Zhang, Y. Wang *et al.*, "Repair of spinal cord injury by implantation of bfgf-incorporated hema-moetacl hydrogel in rats," *Scientific Reports (Nature Publisher Group)*, vol. 5, p. 9017, 2015.

[62] U. Milbreta, L. H. Nguyen, H. Diao, J. Lin, W. Wu, C.-Y. Sun, J. Wang, and S. Y. Chew, "Three-dimensional nanofiber hybrid scaffold directs and enhances axonal regeneration after spinal cord injury," *ACS Biomaterials Science & Engineering*, vol. 2, no. 8, pp. 1319–1329, 2016.

[63] L. H. Nguyen, M. Gao, J. Lin, W. Wu, J. Wang, and S. Y. Chew, "Three-dimensional aligned nanofibers-hydrogel scaffold for controlled non-viral drug/gene delivery to direct axon regeneration in spinal cord injury treatment," *Scientific Reports*, vol. 7, p. 42212, 2017.

[64] C. Ethier, E. R. Oby, M. Bauman, and L. E. Miller, "Restoration of grasp following paralysis through brain-controlled stimulation of muscles," *Nature*, vol. 485, no. 7398, pp. 368–371, 2012.

[65] J. B. Zimmermann and A. Jackson, "Closed-loop control of spinal cord stimulation to restore hand function after paralysis," *Frontiers in neuroscience*, vol. 8, p. 87, 2014.

[66] M. Capogrosso, T. Milekovic, D. Borton, F. Wagner, E. M. Moraud, J.-B. Mignardot, N. Buse, J. Gandar, Q. Barraud, D. Xing *et al.*, "A brain–spine interface alleviating gait deficits after spinal cord injury in primates," *Nature*, vol. 539, no. 7628, pp. 284–288, 2016.

[67] C. E. Bouton, A. Shaikhouni, N. V. Annetta, M. A. Bockbrader, D. A. Friedenberg, D. M. Nielson, G. Sharma, P. B. Sederberg, B. C. Glenn, W. J. Mysiw *et al.*, "Restoring cortical control of functional movement in a human with quadriplegia," *Nature*, vol. 533, no. 7602, pp. 247–250, 2016.

[68] S. Harkema, Y. Gerasimenko, J. Hodes, J. Burdick, C. Angeli, Y. Chen, C. Ferreira, A. Willhite, E. Rejc, R. G. Grossman *et al.*, "Effect of epidural stimulation

of the lumbosacral spinal cord on voluntary movement, standing, and assisted stepping after motor complete paraplegia: a case study," *The Lancet*, vol. 377, no. 9781, pp. 1938–1947, 2011.

[69] A. R. Donati, S. Shokur, E. Morya, D. S. Campos, R. C. Moioli, C. M. Gitti, P. B. Augusto, S. Tripodi, C. G. Pires, G. A. Pereira *et al.*, "Long-term training with a brain-machine interface-based gait protocol induces partial neurological recovery in paraplegic patients," *Scientific reports*, vol. 6, 2016.

[70] J. W. McDonald and C. Sadowsky, "Spinal-cord injury," *The Lancet*, vol. 359, p. 417–425, Feb 2002.

[71] S. N. A., N. Sousa, R. L. Reis, and A. J. Salgado, "From basics to clinical: A comprehensive review on spinal cord injury," *Progress in Neurobiology*, vol. 114, p. 25–57, 2014.

[72] R. Papastefanaki, FlorentiaMatsas, "From demyelination to remyelination : The road toward therapies for spinal cord injury," *Glia*, vol. 63, no. 7, pp. 1101–1125, 2015.

[73] C. A. Oyinbo, "Secondary injury mechanisms in traumatic spinal cord injury: a nugget of this multiply cascade." *Spinal Cord*, vol. 71, pp. 281–299, 2011.

[74] S. Kabu, Y. Gao, B. K. Kwon, and V. Labhasetwar, "Drug delivery, cell-based therapies, and tissue engineering approaches for spinal cord injury," *Journal of Controlled Release*, vol. 219, pp. 141–154, 2015.

[75] J. Y. Tyler, X.-M. Xu, and J.-X. Cheng, "Nanomedicine for treating spinal cord injury," *Nanoscale*, vol. 5, no. 19, pp. 8821–8836, 2013.

[76] A. Faccendini, B. Vigani, S. Rossi, G. Sandri, M. C. Bonferoni, C. M. Caramella, and F. Ferrari, "Nanofiber scaffolds as drug delivery systems to bridge spinal cord injury," *Pharmaceuticals*, vol. 10, no. 3, p. 63, 2017.

[77] S. M. Willerth and S. E. Sakiyama-Elbert, "Approaches to neural tissue engineering using scaffolds for drug delivery," *Advanced drug delivery reviews*, vol. 59, no. 4, pp. 325–338, 2007.

[78] P. Lu, Y. Wang, L. Graham, K. McHale, M. Gao, D. Wu, J. Brock, A. Blesch, E. S. Rosenzweig, L. A. Havton *et al.*, "Long-distance growth and connectivity of neural stem cells after severe spinal cord injury," *Cell*, vol. 150, no. 6, pp. 1264–1273, 2012.

[79] H. Nakajima, K. Uchida, A. R. Guerrero, S. Watanabe, D. Sugita, N. Takeura, A. Yoshida, G. Long, K. T. Wright, W. E. Johnson *et al.*, "Transplantation of mesenchymal stem cells promotes an alternative pathway of macrophage activation and functional recovery after spinal cord injury," *Journal of neurotrauma*, vol. 29, no. 8, pp. 1614–1625, 2012.

[80] J. Sharp, J. Frame, M. Siegenthaler, G. Nistor, and H. S. Keirstead, "Human embryonic stem cell-derived oligodendrocyte progenitor cell transplants improve recovery after cervical spinal cord injury," *Stem cells*, vol. 28, no. 1, pp. 152–163, 2010.

[81] H. Kanno, Y. Pressman, A. Moody, R. Berg, E. M. Muir, J. H. Rogers, H. Ozawa, E. Itoi, D. D. Pearse, and M. B. Bunge, "Combination of engineered schwann cell grafts to secrete neurotrophin and chondroitinase promotes axonal regeneration and locomotion after spinal cord injury," *Journal of Neuroscience*, vol. 34, no. 5, pp. 1838–1855, 2014.

[82] D. D. Pearse, A. R. Sanchez, F. C. Pereira, C. M. Andrade, R. Puzis, Y. Pressman, K. Golden, B. M. Kitay, B. Blits, and P. M. e. a. Wood, "Transplantation of schwann cells and/or olfactory ensheathing glia into the contused spinal cord: Survival, migration, axon association, and functional recovery," *Glia*, vol. 55, no. 9, pp. 976–1000, 2007.

[83] V. Gautam, S. Naureen, N. Shahid, Q. Gao, Y. Wang, D. Nisbet, C. Jagadish, and V. R. Daria, "Engineering highly interconnected neuronal networks on nanowire scaffolds," *Nano letters*, vol. 17, no. 6, pp. 3369–3375, 2017.

[84] P. Timashev, M. Vedunova, D. Guseva, E. Ponimaskin, A. Deiwick, T. Mishchenko, E. Mitroshina, A. Koroleva, A. Pimashkin, I. Mukhina *et al.*, "3d in vitro platform produced by two-photon polymerization for the analysis of neural network formation and function," *Biomedical Physics & Engineering Express*, vol. 2, no. 3, p. 035001, 2016.

[85] T. B. DeMarse, L. Pan, S. Alagapan, G. J. Brewer, and B. C. Wheeler, "Feed-forward propagation of temporal and rate information between cortical populations during coherent activation in engineered in vitro networks," *Frontiers in neural circuits*, vol. 10, p. 32, 2016.

[86] A. Gladkov, Y. Pigareva, D. Kutyina, V. Kolpakov, A. Bukatin, I. Mukhina, V. Kazantsev, and A. Pimashkin, "Design of cultured neuron networks in vitro with predefined connectivity using asymmetric microfluidic channels," *Scientific Reports*, vol. 7, no. 1, p. 15625, 2017.

[87] I. Vismara, S. Papa, F. Rossi, G. Forloni, and P. Veglianese, "Current options for cell therapy in spinal cord injury," *Trends in Molecular Medicine*, vol. 23, no. 9, pp. 831–849, 2017.

[88] F.-M. Chen and X. Liu, "Advancing biomaterials of human origin for tissue engineering," *Progress in polymer science*, vol. 53, pp. 86–168, 2016.

[89] S. Rajangam, P.-H. Tseng, A. Yin, G. Lehew, D. Schwarz, M. A. Lebedev, and M. A. Nicolelis, "Wireless cortical brain-machine interface for whole-body navigation in primates," *Scientific reports*, vol. 6, p. 22170, 2016.

[90] S. Soekadar, M. Witkowski, C. Gómez, E. Opisso, J. Medina, M. Cortese, M. Cempini, M. Carrozza, L. Cohen, N. Birbaumer *et al.*, "Hybrid eeg/eog-based brain/neural hand exoskeleton restores fully independent daily living activities after quadriplegia," *Science Robotics*, vol. 1, no. 1, p. eaag3296, 2016.

[91] K. Ganguly, "An introduction to brain-machine interfaces."

[92] Y. Guo, R. A. Foulds, S. V. Adamovich, and M. Sahin, "Encoding of forelimb forces by corticospinal tract activity in the rat," *Frontiers in neuroscience*, vol. 8, 2014.

[93] N. J. Hill, D. Gupta, P. Brunner, A. Gunduz, M. A. Adamo, A. Ritaccio, and G. Schalk, "Recording human electrocorticographic (ecog) signals for neuroscientific research and real-time functional cortical mapping," *JoVE (Journal of Visualized Experiments)*, no. 64, pp. e3993–e3993, 2012.

[94] G. Schalk and E. C. Leuthardt, "Brain-computer interfaces using electrocorticographic signals," *IEEE reviews in biomedical engineering*, vol. 4, pp. 140–154, 2011.

[95] W. Wang, A. D. Degenhart, J. L. Collinger, R. Vinjamuri, G. P. Sudre, P. D. Adelson, D. L. Holder, E. C. Leuthardt, D. W. Moran, M. L. Boninger *et al.*, "Human motor cortical activity recorded with micro-ecog electrodes, during individual finger movements," in *Engineering in Medicine and Biology Society, 2009. EMBC 2009. Annual International Conference of the IEEE.* IEEE, 2009, pp. 586–589.

[96] Z. C. Chao, Y. Nagasaka, and N. Fujii, "Long-term asynchronous decoding of arm motion using electrocorticographic signals in monkey," *Frontiers in neuroengineering*, vol. 3, p. 3, 2010.

[97] G. Hotson, D. P. McMullen, M. S. Fifer, M. S. Johannes, K. D. Katyal, M. P. Para, R. Armiger, W. S. Anderson, N. V. Thakor, B. A. Wester *et al.*, "Individual finger control of a modular prosthetic limb using high-density electrocorticography in a human subject," *Journal of neural engineering*, vol. 13, no. 2, p. 026017, 2016.

[98] S. Gok and M. Sahin, "Prediction of forelimb muscle emgs from the corticospinal signals in rats," in *Engineering in Medicine and Biology Society (EMBC), 2016 IEEE 38th Annual International Conference of the.* IEEE, 2016, pp. 2780–2783.

[99] L. F. Nicolas-Alonso and J. Gomez-Gil, "Brain computer interfaces, a review," *Sensors*, vol. 12, no. 2, pp. 1211–1279, 2012.

[100] M. D. Serruya, N. G. Hatsopoulos, L. Paninski, M. R. Fellows, and J. P. Donoghue, "Brain-machine interface: Instant neural control of a movement signal," *Nature*, vol. 416, no. 6877, pp. 141–142, 2002.

[101] D. M. Taylor, S. I. H. Tillery, and A. B. Schwartz, "Direct cortical control of 3d neuroprosthetic devices," *Science*, vol. 296, no. 5574, pp. 1829–1832, 2002.

[102] P. R. Kennedy, R. A. Bakay, M. M. Moore, K. Adams, and J. Goldwaithe, "Direct control of a computer from the human central nervous system," *IEEE Transactions on rehabilitation engineering*, vol. 8, no. 2, pp. 198–202, 2000.

[103] S. Musallam, B. Corneil, B. Greger, H. Scherberger, and R. Andersen, "Cognitive control signals for neural prosthetics," *Science*, vol. 305, no. 5681, pp. 258–262, 2004.

[104] L. R. Hochberg, M. D. Serruya, G. M. Friehs, J. A. Mukand, M. Saleh, A. H. Caplan, A. Branner, D. Chen, R. D. Penn, and J. P. Donoghue, "Neuronal ensemble control of prosthetic devices by a human with tetraplegia," *Nature*, vol. 442, no. 7099, pp. 164–171, 2006.

[105] J. Simeral, S.-P. Kim, M. Black, J. Donoghue, and L. Hochberg, "Neural control of cursor trajectory and click by a human with tetraplegia 1000 days after implant of an intracortical microelectrode array," *Journal of neural engineering*, vol. 8, no. 2, p. 025027, 2011.

[106] L. R. Hochberg, D. Bacher, B. Jarosiewicz, N. Y. Masse, J. D. Simeral, J. Vogel, S. Haddadin, J. Liu, S. S. Cash, P. van der Smagt *et al.*, "Reach and grasp by people with tetraplegia using a neurally controlled robotic arm," *Nature*, vol. 485, no. 7398, pp. 372–375, 2012.

[107] J. L. Collinger, B. Wodlinger, J. E. Downey, W. Wang, E. C. Tyler-Kabara, D. J. Weber, A. J. McMorland, M. Velliste, M. L. Boninger, and A. B. Schwartz, "High-performance neuroprosthetic control by an individual with tetraplegia," *The Lancet*, vol. 381, no. 9866, pp. 557–564, 2013.

[108] M. Velliste, S. Perel, M. C. Spalding, A. S. Whitford, and A. B. Schwartz, "Cortical control of a prosthetic arm for self-feeding," *Nature*, vol. 453, no. 7198, pp. 1098–1101, 2008.

[109] C. T. Moritz, S. I. Perlmutter, and E. E. Fetz, "Direct control of paralysed muscles by cortical neurons," *Nature*, vol. 456, no. 7222, pp. 639–642, 2008.

[110] E. A. Pohlmeyer, E. R. Oby, E. J. Perreault, S. A. Solla, K. L. Kilgore, R. F. Kirsch, and L. E. Miller, "Toward the restoration of hand use to a paralyzed monkey: brain-controlled functional electrical stimulation of forearm muscles," *PloS one*, vol. 4, no. 6, p. e5924, 2009.

[111] V. Caggiano, M. Sur, and E. Bizzi, "Rostro-caudal inhibition of hindlimb movements in the spinal cord of mice," *PloS one*, vol. 9, no. 6, p. e100865, 2014.

[112] V. Caggiano, V. C. Cheung, and E. Bizzi, "An optogenetic demonstration of motor modularity in the mammalian spinal cord," *Scientific reports*, vol. 6, p. 35185, 2016.

[113] K. L. Montgomery, S. M. Iyer, A. J. Christensen, K. Deisseroth, and S. L. Delp, "Beyond the brain: Optogenetic control in the spinal cord and peripheral nervous system," *Science translational medicine*, vol. 8, no. 337, pp. 337rv5–337rv5, 2016.

[114] S. I. Park, D. S. Brenner, G. Shin, C. D. Morgan, B. A. Copits, H. U. Chung, M. Y. Pullen, K. N. Noh, S. Davidson, S. J. Oh *et al.*, "Soft, stretchable, fully implantable miniaturized optoelectronic systems for wireless optogenetics," *Nature biotechnology*, vol. 33, no. 12, p. 1280, 2015.

[115] K. L. Montgomery, A. J. Yeh, J. S. Ho, V. Tsao, S. M. Iyer, L. Grosenick, E. A. Ferenczi, Y. Tanabe, K. Deisseroth, S. L. Delp *et al.*, "Wirelessly powered, fully internal optogenetics for brain, spinal and peripheral circuits in mice," *Nature methods*, vol. 12, no. 10, pp. 969–974, 2015.

[116] M. J. Weber, A. Bhat, T. C. Chang, J. Charthad, and A. Arbabian, "A miniaturized ultrasonically powered programmable optogenetic implant stimulator system," in *Biomedical Wireless Technologies, Networks, and Sensing Systems (BioWireleSS), 2016 IEEE Topical Conference on*. IEEE, 2016, pp. 12–14.

[117] A. Arbabian, T. C. Chang, M. L. Wang, J. Charthad, S. Baltsavias, M. Fallahpour, and M. J. Weber, "Sound technologies, sound bodies: Medical implants with ultrasonic links," *IEEE Microwave Magazine*, vol. 17, no. 12, pp. 39–54, 2016.

[118] K. C. Larsson, P. Kjäll, and A. Richter-Dahlfors, "Organic bioelectronics for electronic-to-chemical translation in modulation of neuronal signaling and machine-to-brain interfacing," *Biochimica et Biophysica Acta (BBA)-General Subjects*, vol. 1830, no. 9, pp. 4334–4344, 2013.

[119] C. Ghez, J. Gordon, M. Ghilardi, C. Christakos, and S. E. Cooper, "Roles of proprioceptive input in the programming of arm trajectories," in *Cold spring harbor symposia on quantitative biology*, vol. 55. Cold Spring Harbor Laboratory Press, 1990, pp. 837–847.

[120] A. J. Suminski, D. C. Tkach, A. H. Fagg, and N. G. Hatsopoulos, "Incorporating feedback from multiple sensory modalities enhances brain–machine interface control," *Journal of Neuroscience*, vol. 30, no. 50, pp. 16 777–16 787, 2010.

[121] R. C. Rollings, A. T. Kuan, and J. A. Golovchenko, "Ion selectivity of graphene nanopores," *Nature communications*, vol. 7, 2016.

[122] D. C. Elias, R. R. Nair, T. Mohiuddin, S. Morozov, P. Blake, M. Halsall, A. Ferrari, D. Boukhvalov, M. Katsnelson, A. Geim *et al.*, "Control of graphene's properties by reversible hydrogenation: evidence for graphane," *Science*, vol. 323, no. 5914, pp. 610–613, 2009.

[123] R. R. Nair, W. Ren, R. Jalil, I. Riaz, V. G. Kravets, L. Britnell, P. Blake, F. Schedin, A. S. Mayorov, S. Yuan *et al.*, "Fluorographene: A two-dimensional counterpart of teflon," *small*, vol. 6, no. 24, pp. 2877–2884, 2010.

[124] J. Zhang *et al.*, "Communication channel analysis and real time compressed sensing for high density neural recording devices," *IEEE Transactions on Circuits and Systems*, vol. 63, no. 5, pp. 599–608, 2016.

[125] S. Kim *et al.*, "Preliminary study of the thermal impact of a microelectrode array implanted in the brain," in *Proceedings of the 28th IEEE EMBS Annual International Conference*. IEEE, Aug. 2006.

[126] K. Abdelhalim, H. M. Jafari, L. Kokarovtseva, J. L. P. Velazquez, and R. Genov, "64-channel uwb wireless neural vector analyzer soc with a closed-loop phase synchrony-triggered neurostimulator," *IEEE Journal of Solid-State Circuits*, vol. 48, no. 10, pp. 2494–2510, Oct 2013.

[127] O. Novak, W. Wu, and C. Charles, "Wireless ultra-wide-band data link for biomedical implants," in *2009 Ph.D. Research in Microelectronics and Electronics*, July 2009, pp. 352–355.

[128] K. M. S. Thotahewa, J. Y. Khan, and M. R. Yuce, "Power efficient ultra wide band based wireless body area networks with narrowband feedback path," *IEEE Transactions on Mobile Computing*, vol. 13, no. 8, pp. 1829–1842, Aug 2014.

[129] J. Zhang, K. Duncan, Y. Suo, T. Xiong, S. Mitra, T. D. Tran, and R. Etienne-Cummings, "Communication channel analysis and real time compressed sensing

for high density neural recording devices," *IEEE Transactions on Circuits and Systems I: Regular Papers*, vol. 63, no. 5, pp. 599–608, May 2016.

[130] H. Ando, K. Takizawa, T. Yoshida, K. Matsushita, M. Hirata, and T. Suzuki, "Wireless multichannel neural recording with a 128-mbps uwb transmitter for an implantable brain-machine interfaces," *IEEE Transactions on Biomedical Circuits and Systems*, vol. 10, no. 6, pp. 1068–1078, Dec 2016.

[131] S. Kabiri Ameri, R. Ho, H. Jang, L. Tao, Y. Wang, L. Wang, D. M. Schnyer, D. Akinwande, and N. Lu, "Graphene electronic tattoo sensors," *ACS nano*, vol. 11, no. 8, pp. 7634–7641, 2017.

[132] S. Lim, D. Son, J. Kim, Y. B. Lee, J.-K. Song, S. Choi, D. J. Lee, J. H. Kim, M. Lee, T. Hyeon *et al.*, "Transparent and stretchable interactive human machine interface based on patterned graphene heterostructures," *Advanced Functional Materials*, vol. 25, no. 3, pp. 375–383, 2015.

[133] M. Kang, J. Kim, B. Jang, Y. Chae, J.-H. Kim, and J.-H. Ahn, "Graphene-based three-dimensional capacitive touch sensor for wearable electronics," *ACS nano*, vol. 11, no. 8, pp. 7950–7957, 2017.

[134] Q. Zhang, L. Tan, Y. Chen, T. Zhang, W. Wang, Z. Liu, and L. Fu, "Human-like sensing and reflexes of graphene-based films," *Advanced Science*, vol. 3, no. 12, 2016.

[135] H.-L. C. Kao, C. Holz, A. Roseway, A. Calvo, and C. Schmandt, "Duoskin: rapidly prototyping on-skin user interfaces using skin-friendly materials," in *Proceedings of the 2016 ACM International Symposium on Wearable Computers*. ACM, 2016, pp. 16–23.

[136] X. Huang, T. Leng, X. Zhang, J. C. Chen, K. H. Chang, A. K. Geim, K. S. Novoselov, and Z. Hu, "Binder-free highly conductive graphene laminate for low cost printed radio frequency applications," *Applied Physics Letters*, vol. 106, no. 20, p. 203105, 2015.

[137] D. Seo, R. M. Neely, K. Shen, U. Singhal, E. Alon, J. M. Rabaey, J. M. Carmena, and M. M. Maharbiz, "Wireless recording in the peripheral nervous system with ultrasonic neural dust," *Neuron*, vol. 91, no. 3, pp. 529–539, 2016.

[138] G. E. Santagati and T. Melodia, "Experimental evaluation of impulsive ultrasonic intra-body communications for implantable biomedical devices," *IEEE Transactions on Mobile Computing*, vol. 16, no. 2, pp. 367–380, 2017.

[139] S. Wilson and C. Moore, "S1 somatotopic maps," *Scholarpedia*, vol. 10, no. 4, p. 8574, 2015, revision #150585.

[140] S. N. Flesher, J. L. Collinger, S. T. Foldes, J. M. Weiss, J. E. Downey, E. C. Tyler-Kabara, S. J. Bensmaia, A. B. Schwartz, M. L. Boninger, and R. A. Gaunt, "Intracortical microstimulation of human somatosensory cortex," *Science translational medicine*, vol. 8, no. 361, pp. 361ra141–361ra141, 2016.

[141] S. J. Bensmaia, "Biological and bionic hands: natural neural coding and artificial perception," *Phil. Trans. R. Soc. B*, vol. 370, no. 1677, p. 20140209, 2015.

[142] F. Xu, H. Yu, A. Sadrzadeh, and B. I. Yakobson, "Riemann surfaces of carbon as graphene nanosolenoids," *Nano letters*, vol. 16, no. 1, pp. 34–39, 2015.

[143] S. P. Beeby, M. J. Tudor, and N. White, "Energy harvesting vibration sources for microsystems applications," *Measurement science and technology*, vol. 17, no. 12, p. R175, 2006.